UCID- 21493

Source Near-Field Effects on HPM Coupling

R. J. King
H. G. Hudson

August 1988

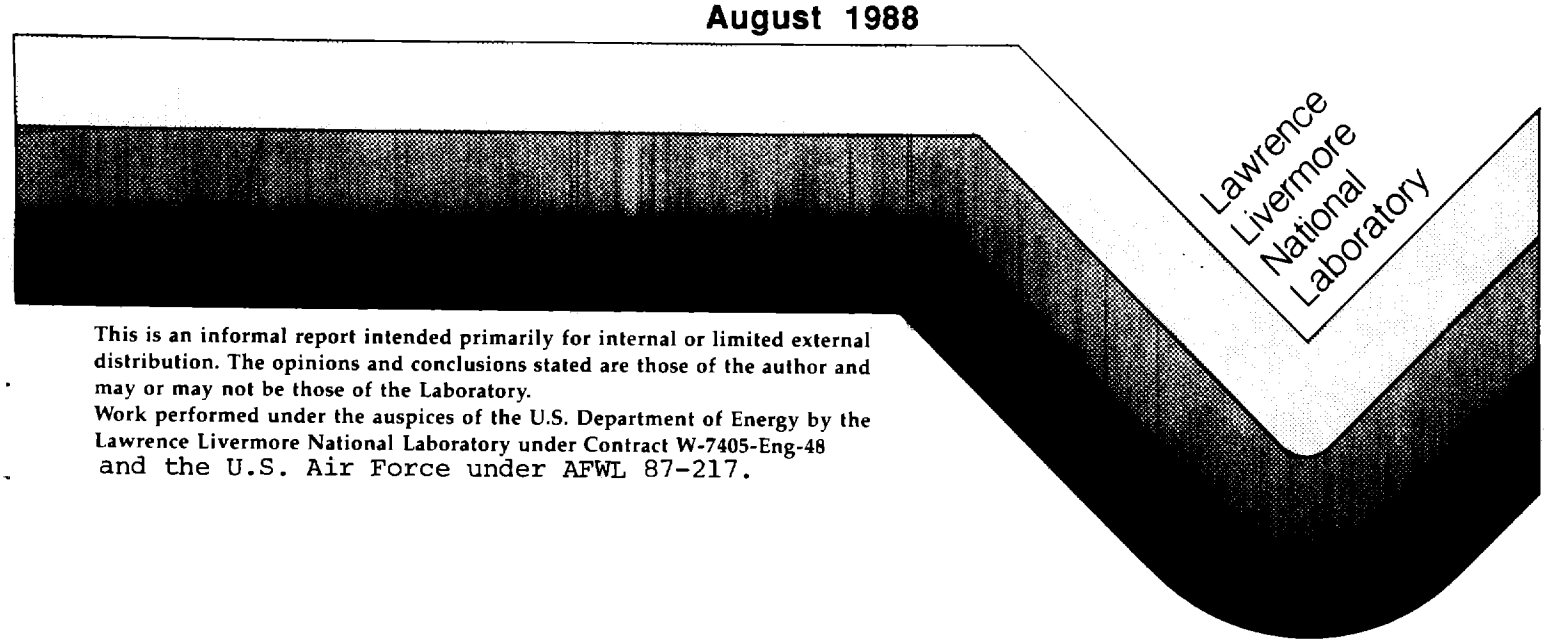

Work performed under the auspices of the U.S. Department of Energy by the Lawrence Livermore National Laboratory under Contract W-7405-Eng-48 and the U.S. Air Force under AFWL 87-217.

Printed in the United States of America
Available from
National Technical Information Service
U.S. Department of Commerce
5285 Port Royal Road
Springfield, VA 22161

Price Code	Page Range
A01	Microfiche
Papercopy Prices	
A02	001 - 050
A03	051 - 100
A04	101 - 200
A05	201 - 300
A06	301 - 400
A07	401 - 500
A08	501 - 600
A09	601

Table of Contents

Acknowledgements:

We gratefully acknowledge the encouragement by Dr. Hriar S. Cabayan to embark on this study and his constructive suggestions during its progress. The financial support by the Air Force Weapons Laboratory through Lt. Col. John A. Demarest is gratefully appreciated. We also thank Mr. Dan Gnade for designing and constructing the test objects, and for his careful attention to carrying out the laboratory experiments. Finally, we thank Gretchen Dodd for typing this report.

Executive Summary

When testing full systems in HPM simulators, there may be need to conduct the tests in the near-field of the source antenna in order to obtain high incident fluences. In doing so, only a few ports of entry (POEs) may be illuminated at the same time. This leads to the need to address several important issues:

(a) What is the near-field structure (i.e, columnation, spot size and polarization purity) of the source antenna and how does it affect coupling?
(b) Are there significant mutual interactions between the source antenna and the test system? Between the POEs within the test system?
(c) Does near-field receiving cross-section have meaning, and if so, how does it compare with the far-field cross section?
(d) Can near-field tests on individual POEs be superimposed to predict the coupling response to plane wave (far-field) illumination of multiple POEs?
(e) Which are the most important POEs and at what frequencies are they important?
(f) How does the phase front of an incident wave contribute to coupling via multiple POEs?
(g) How do the angle and polarization of the incident wave effect coupling for one vs several open POEs?

This report gives an overview of many of these issues and sites examples. It is part of an on-going effort to investigate all aspects of the phenomenology of HPM interactions with systems. Experimental results are given for near-field coupling into generic test systems. While we do not exhaustively answer all of these questions, certain trends are observed. From these, some general conclusions are drawn to guide the use of HPM simulators for testing full systems.

The results of this study clearly point to the need for low level cw characterization of a test system in order to understand the roles that each of several POEs can play. The frequencies at which each POE contributes is particularly important. The dependence on the incidence angle is also important but to a lesser degree over certain sectors, depending on the POE receiving pattern which is often quite broad. Low level characterization allows one to show how the near-field coupling compares to far-field coupling, thereby giving insight into the approximations and risks taken in placing the test object in the near-field of

an HPM source. The source antenna should also be characterized to determine its antenna factor vs frequency, and to ensure that its near-field is properly shaped and polarized.

The near- and far-field receiving cross section compared quite favorably, provided that the near-field spot size is large enough to illuminate all of the important POEs simultaneously. Near-field cross sections can be calculated in the same manner as is usually done for far-field illumination.

For multiple POEs, coupling is comprised of two parts: a deterministic part (generally resulting from the coherent contributions of a few dominant POEs), and a more or less stochastic part (resulting from the incoherent contributions of several lessor contributing POEs) superimposed on the deterministic part. At frequencies, angles of incidence or polarization where the deterministic part is well-behaved (e.g., when there is only one dominant POE), the average of the true far-field cross section is well approximated as the scalar sum of the near-field cross sections, $\Sigma\sigma_n$. Such a scalar sum, however, obviously cannot account for the details of constructive interferences which may happen when two or more POEs are dominant. Thus, if the phase of the incident field deviates from that of a plane wave, the coupling details become blurred, but the trend is relatively unchanged. If only the response trend is sufficient, the incoherent sum $\Sigma\sigma_n$ resulting from near-field testing is adequate.

Coupling to a single POE is generally quite insensitive to the angle of incidence over wide angular sectors. For multiple POEs having nearly equal contributions, coupling becomes highly deterministic and coherent. In a real system this is an unlikely situation. But if it does occur, strong interferences can be observed. Again, if all of the important POEs of such a system are illuminated by the near-field of a source antenna, these interferences become blurred.

Filling an object with hardware, compared to when the same object is empty, reduces the average coupling, especially at the higher frequencies. This attenuation is proportional to the distance from the POE to the measurement terminal. Fill also has the effect of smoothing the coupling response vs frequency, i.e., the Q-factors of the resonances are substantially reduced. Since the resonances are damped by the fill, the impact of additional blurring caused by placing the object in the source near-field is diminished.

1. Introduction

In order to achieve maximum intensity of an HPM field incident on a target test system, the HPM source antenna (typically a YAGGI or a horn) is brought within a few feet of the system. Locating the test system in the near-field of the source antenna is clearly not equivalent to illuminating it with a plane wave. This then raises a number of questions about how well such near-field tests simulate a more realistic far-field test, i.e., when the target is illuminated by a plane wave.

First, there is the question of illumination spot size, i.e., how many of the ports-of-entry (POEs) are excited? Related questions pertain to determining which POEs dominate coupling into the system interior, the frequencies, polarization and incidence angles at which they do so, and how the phasing of the incident field affect coupling via the most important POEs.

When characterizing the electromagnetic coupling from the exterior to a specified interior point (terminal), an important parameter is the receiving cross-section

$$\sigma = P_L/S_{inc}, \quad \text{sq. meters} \tag{1}$$

where P_L is the power delivered to a load (typically 50 Ω, corresponding to the input impedance of a measuring instrument) and S_{inc} is the incident power density. Thus, σ provides a direct measure of power available to a known load, given the incident power density. S_{inc} is well known in the case of an incident plane wave,

$$S_{inc} = \frac{|E_{inc}|^2}{\eta_0} = \eta_0 |H_{inc}|^2 \quad , \tag{2}$$

but such is not the case when the coupling object is located in the source near-field. Thus, the question is posed whether the field measured on boresight in the near-field of the source antenna can be used in (2) and (1) in order to compute σ and how well such a calculation compares to the more traditional far-field calculation.

Results which address these effects are given here using a large generic test object having multiple POEs. This object is configured with three interior bulkheads and two coupling wires running from end to end. Data taken when the object is empty are

compared with that when it is filled with random pieces of electronic hardware. These data were taken in the frequency range of 0.5 $\rightarrow$ 2 GHz which is the design frequency band of the source horn antenna used. Although chief attention is focused on response amplitudes, the actual measured data does include phase as well. Consequently, it is possible to sum the complex contributions of individual POEs and thereby reconstruct phasor sums which describe the actual total coupling process.

All of the experimental data given here were taken at low power levels. Consequently, non-linear effects (e.g., aperture breakdown and non-linearity of circuits) are not included.

The present study complements a preliminary study by Toth and Bacon [1], which used a highly deterministic test object over a more restricted frequency range (2 $\rightarrow$ 4 GHz). An abbreviated version of the present study is given in [2].

2. Source Antenna Characterization

Before any meaningful near-field coupling assessments can be made, it is essential to characterize the source antenna itself. The antenna used in these studies was an EMCO Model 3106, shown in Fig. 2.1. This horn is linearly polarized across the small dimension (Fig. 2.2), and normally operates in the frequency band of .5 → 2 GHz.

Numerous measurements of the six field components ($E_{x,y,z}$ and $H_{x,y,z}$) were made across the horn aperture at distances from the aperture ranging from 1 to 15 ft. These measurements revealed that the polarization retained a high degree of fidelity, i.e., the main components were E_x and H_y, all others being of the order of 25 dB or more below the main components.

The antenna receiving factor, defined as

$$F_A(f) = \frac{V_L(f)}{E_{inc}(f)} \quad \text{meters} \tag{3}$$

was measured vs. frequency f, from 45 MHz to 4 GHz (Fig. 2.3) on the LLNL EMPEROR Facility [3] for boresight illumination by the incident field, E_{inc}. Here, $V_L(f)$ is the measured voltage at the 50 ohm impedance of the network analyzer used in the measurement. The data in Fig. 2.3 shows that the antenna has maximum response at .5 GHz, and the response tapers off gradually up to 4 GHz. At 2 GHz, the receiving factor is down about 9 dB. This, and the fact that the baluns on the field sensors used to characterize the near-field perform satisfactorily up to 2 GHz, set the overall frequency range at 0.5 → 2 GHz for these studies.

Figs. 2.4 and 2.5 show the behavior of the E_x and H_y fields respectively, versus distance from the horn aperture at 0.5, 1 and 2 GHz. For comparison, the inverse distance factor r^{-1} is also shown. In these figures, the reference (i.e., zero dB) is at 15 ft. It is clearly evident that the fields increase less rapidly than r^{-1} as r decreases, for all frequencies.

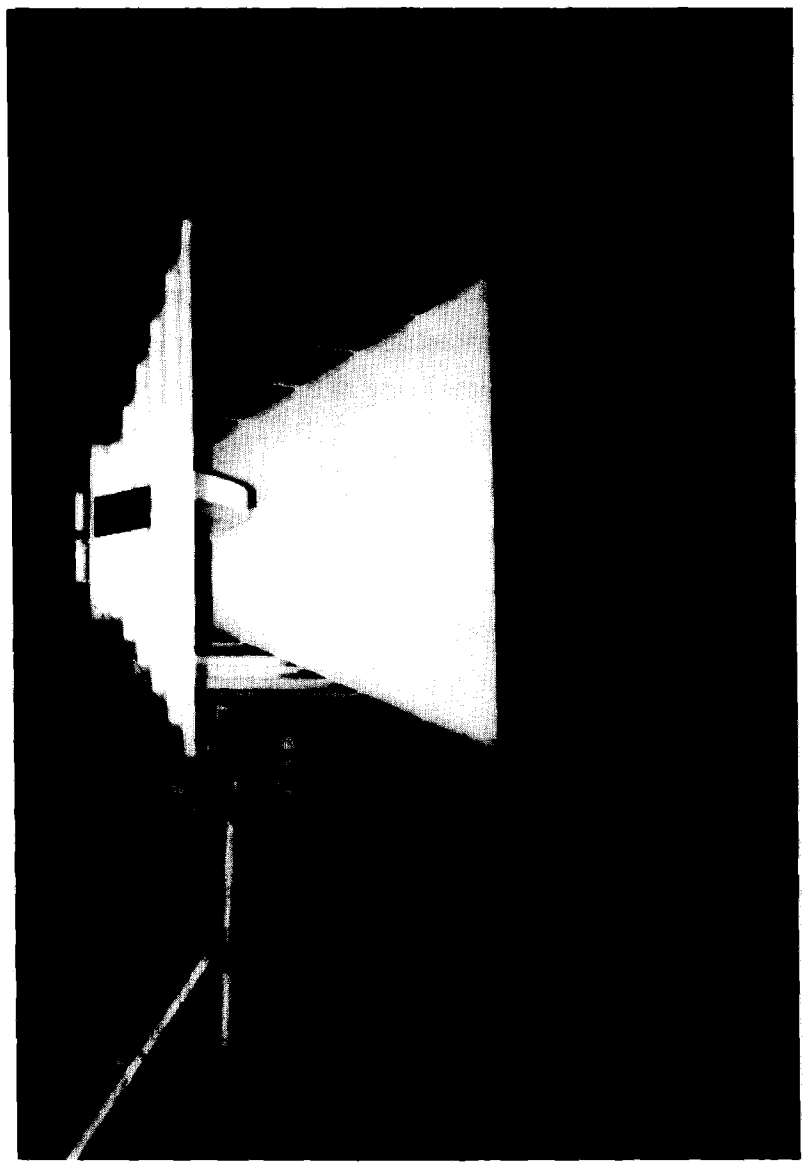

Fig. 2.1 Photograph of the EMCO Model 3106 Antenna used in this study.

Similar data are given in Figs. 2.6 and 2.7, which shows the boresight E_x and H_y fields respectively, versus frequency. These data are given for r = 1, 3 and 6 ft. relative to the fields at r_o = 15 ft. (zero dB). The horizontal lines in Figs. 2.6 and 2.7 show what the respective fields would be if their intensity were to vary as r^{-1}. The fact that these fields are below the horizontal lines also shows that they increase more slowly than r^{-1} as the observer approaches the horn aperture. Irregular features which are particularly apparent

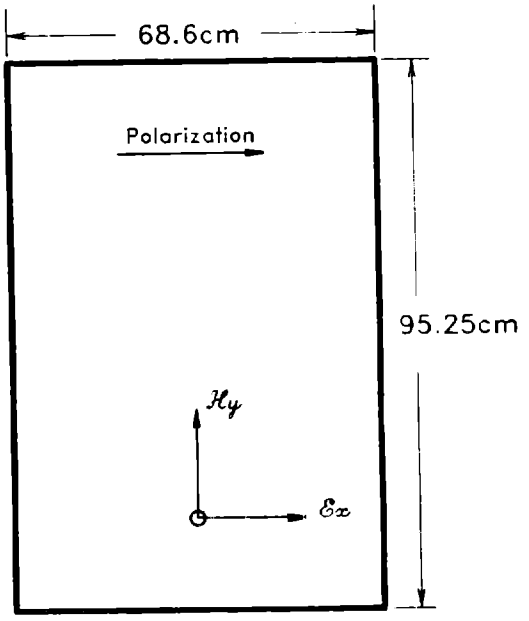

Fig. 2.2. Aperture dimensions and polarization of the EMCO 3106 horn antenna shown in Fig. 2.1.

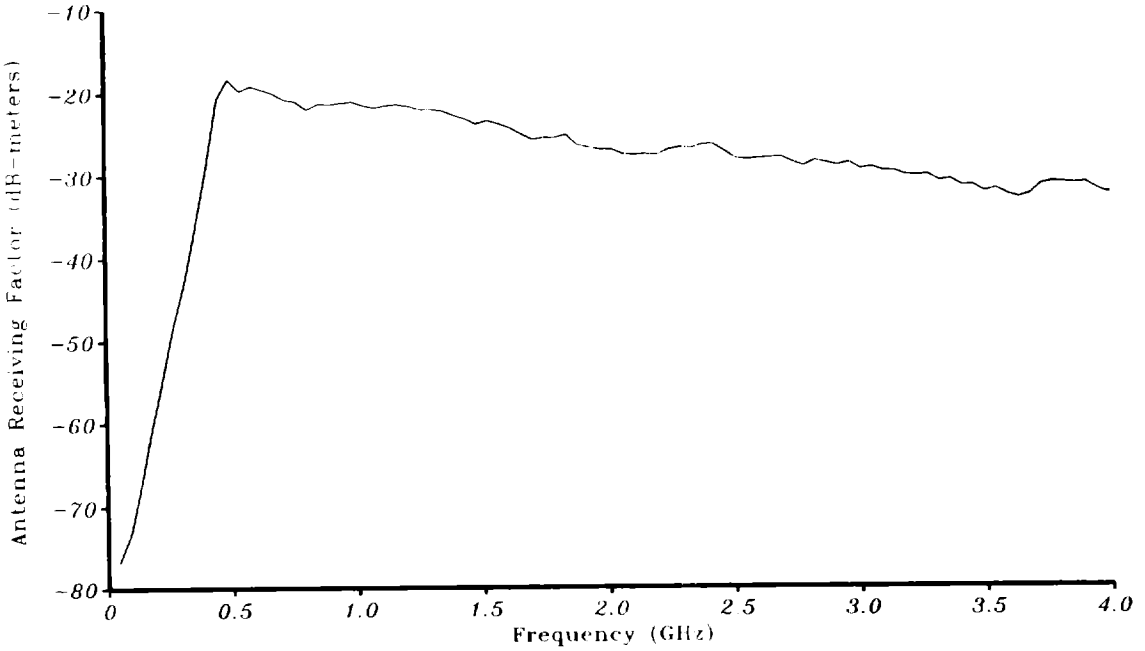

Fig. 2.3. Antenna receiving factor amplitude for the EMCO 3106 horn antenna.

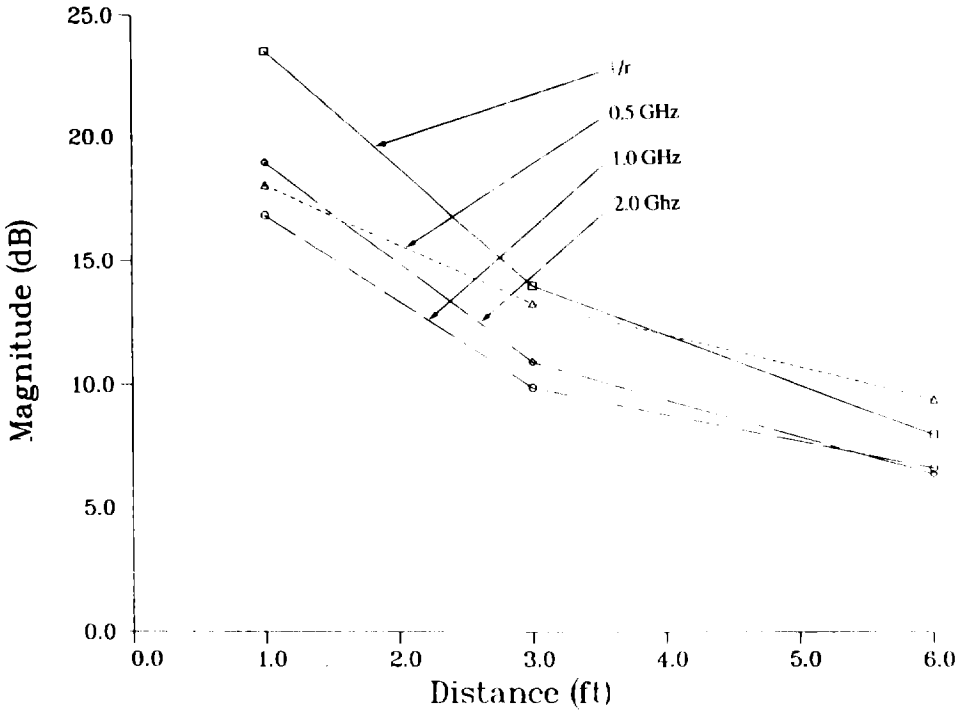

Fig. 2.4. Boresight intensity of E_x. Zero db is at 15 ft.

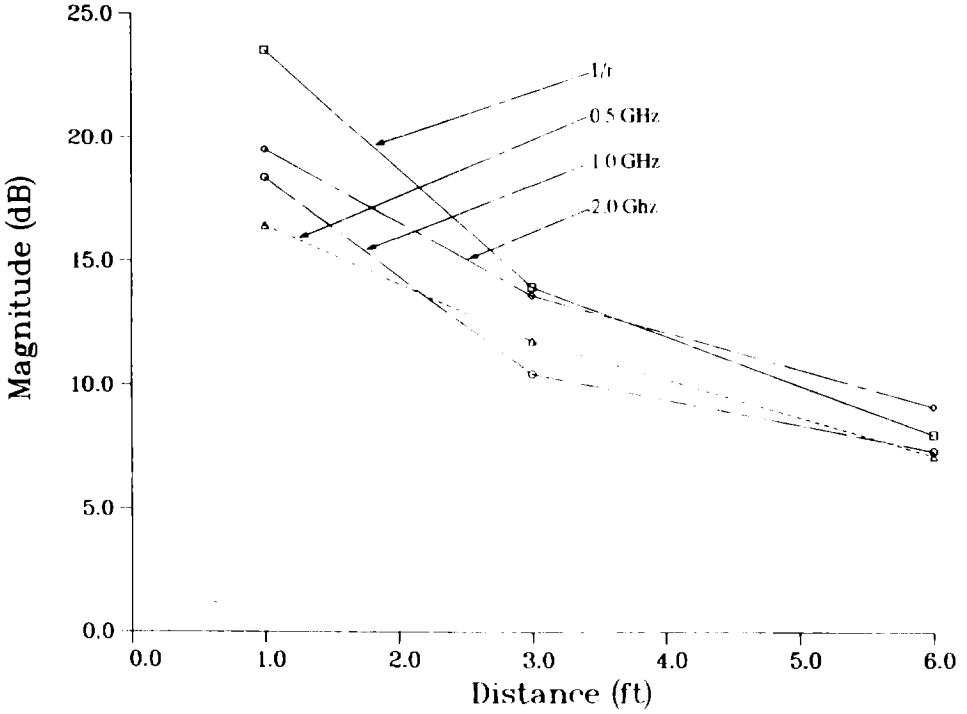

Fig. 2.5. Boresight intensity of H_y. Zero dB is at 15 ft.

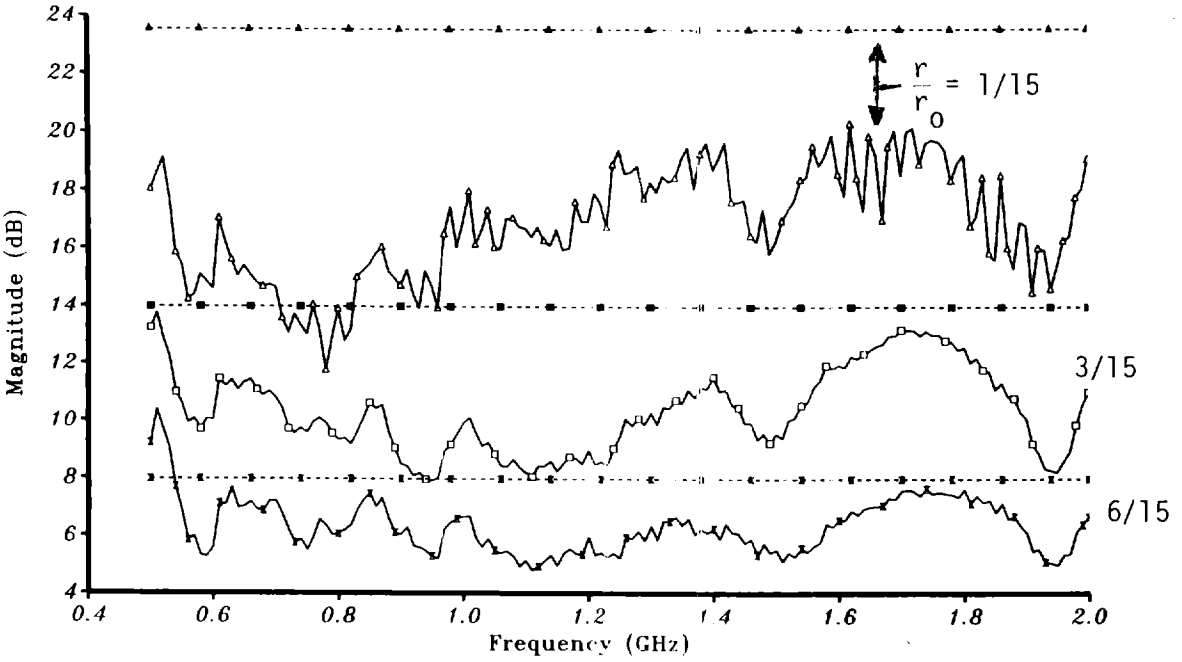

Fig. 2.6. Near-field structure of the $E_x(f)$ field on boresight, relative to that at r_0 = 15 ft. (zero dB) for r = 1, 3, and 6 ft.

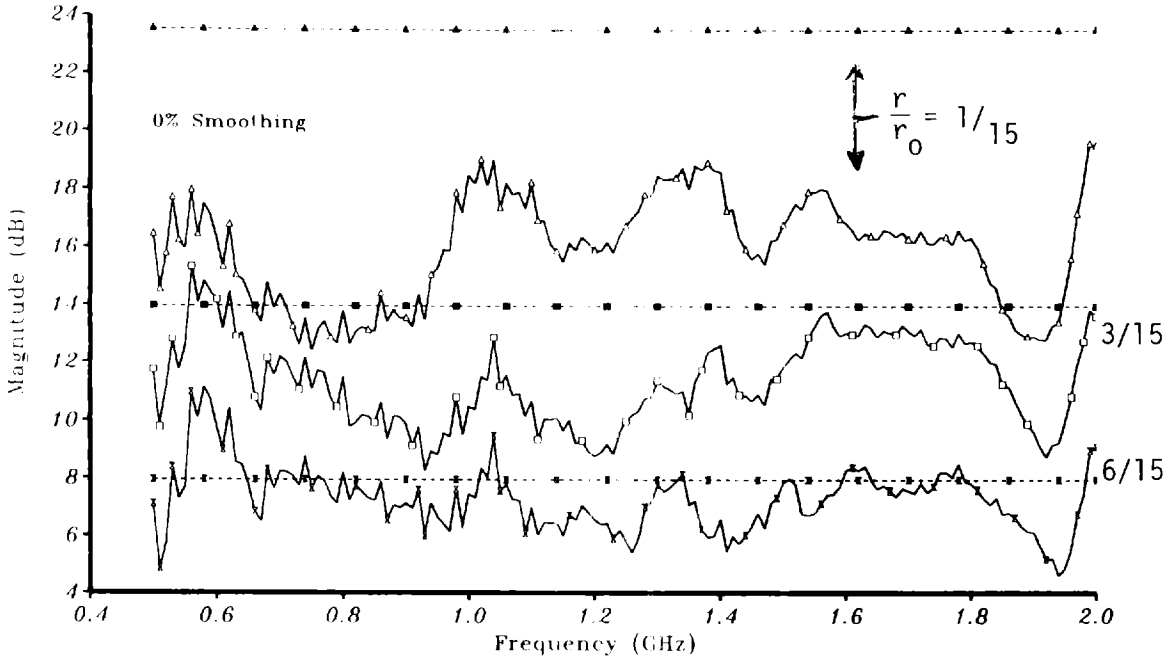

Fig. 2.7. Near-field structure of the $H_y(f)$ field on boresight, relative to that at r_0 = 15 ft. (zero dB) for r = 1. 3, and 6 ft.

for E_x and $r/r_o = 1/15$ suggests substantial variations in the reactive field very near the source antenna aperture, i.e., at r = 1 ft. These near-field variations quickly subside with increasing distance, as expected.

E-plane radiation patterns for the horn antenna are shown in Figs. 2.8 and 2.9, corresponding to r = 3 and 15 ft. respectively, for .5, .75, 1 and 2 GHz. Here, it is seen that the beamwidth generally increases with frequency, an effect which would normally not be expected for a horn antenna. This, however, is consistent with the fact that the antenna far-field receiving factor is maximum at 0.5 GHz as seen in Fig. 2.3.

When an obstruction is placed in the foreground of the horn aperture, power is reflected back into the horn feed, thereby tending to reduce the net transmitted power. Since the test object used here is large and metallic, and will be placed within one foot of the horn aperture, it is of interest to quantify the resulting reduction of net transmitted power. This was accomplished by measuring the s_{11} scattering parameter at the horn input over the $0.5 \rightarrow 2$ GHz frequency range. The fractional power transmitted into the horn input is then

$$P_t = 1 - |s_{11}|^2 \tag{4}$$

Fig. 2.10 shows the results of such measurements, plotted in dB where zero dB represents 100% power transmission. Here, three cases as depicted on the right are compared. The first, which is represented by triangles in Fig. 2.10, is the power transmitted into the horn with no obstruction in the aperture foreground, i.e., the horn is faced toward an absorbing wall of the anechoic chamber. The second case, which is represented by rectangles, is when the large metal test object of this study (see Fig. 3.1) is placed one foot from the horn aperture at broadside incidence. The third and worst case, which is represented by the dotted curve in Fig. 2.10, is when the horn is aimed directly at a metal ground plane located one foot from the horn aperture at broadside incidence. In the second and third cases, the periodic structure of the net transmitted power is due to multiple reflections (mutual interactions) between the reflecting object and the horn itself. Fig. 2.11 is the same data as in Fig. 2.10, except that cases 2 and 3 are normalized by that of case 1. Thus, these data represent just the perturbing effect of mutual interactions between the reflecting object and the horn.

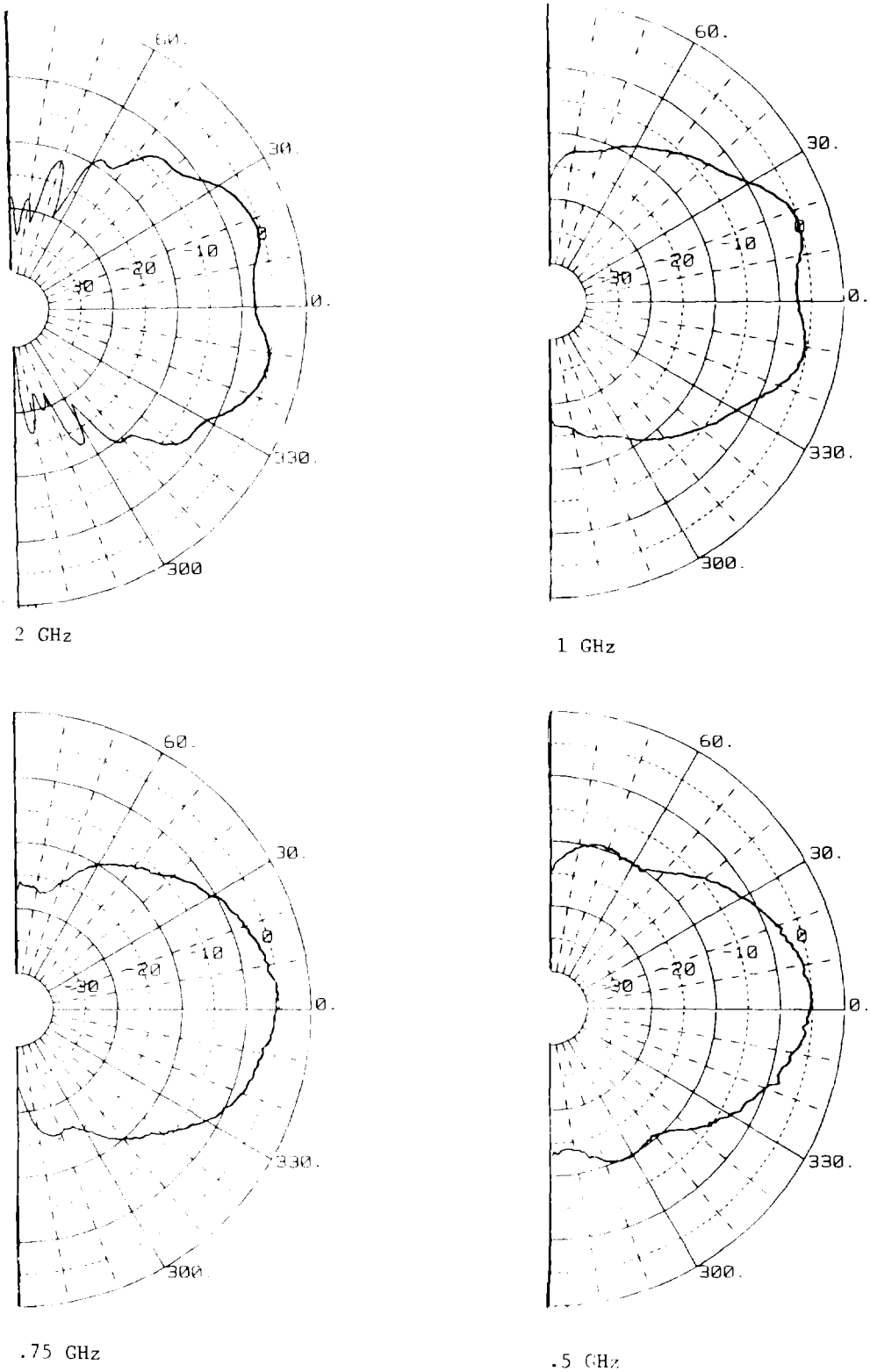

Fig. 2.8. E-Plane transmitting pattern of the EMCO 3106 Horn Antenna measured at 3 ft. from the horn aperture.

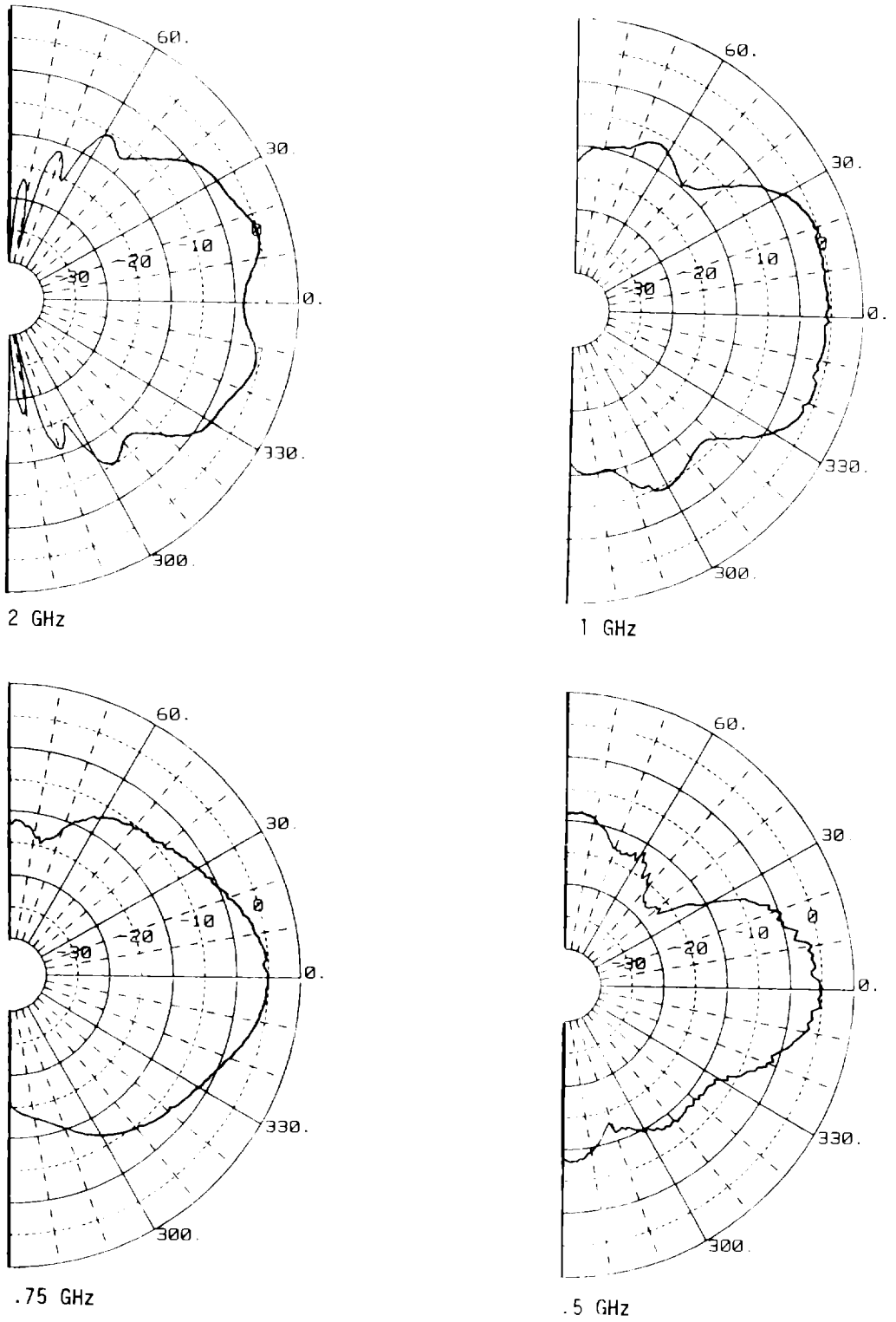

Fig. 2.9. E-Plane transmitting pattern of the EMCO 3106 Horn Antenna measured at 15 ft. from the horn aperture.

From Fig. 2.11, it is seen that the effects of mutual interactions are only about 1 dB in the worst case where the horn is one foot from the reflecting ground plane, and only about 0.5 dB when the large metallic reflecting object is one foot from the horn aperture. From these data, it can be argued that variations of the net field incident on the test object are less than 0.5 dB when the object is located as close as one foot from the horn aperture, and even less when the object and the horn are further removed from each other. Thus, the free-field of the horn (in the absence of the reflecting object) very nearly represents the incident field on the test object. From the results shown in Figs. 2.3 - 2.11, the near-fields on boresight in the immediate foreground of the aperture are seen to be relatively well-behaved with no surprises. In subsequent calculations for the receiving cross section of the test object using Eq. (2), the incident field will therefore be taken as that measured in the absence of the object. This assumption is accurate within 0.5 dB or less.

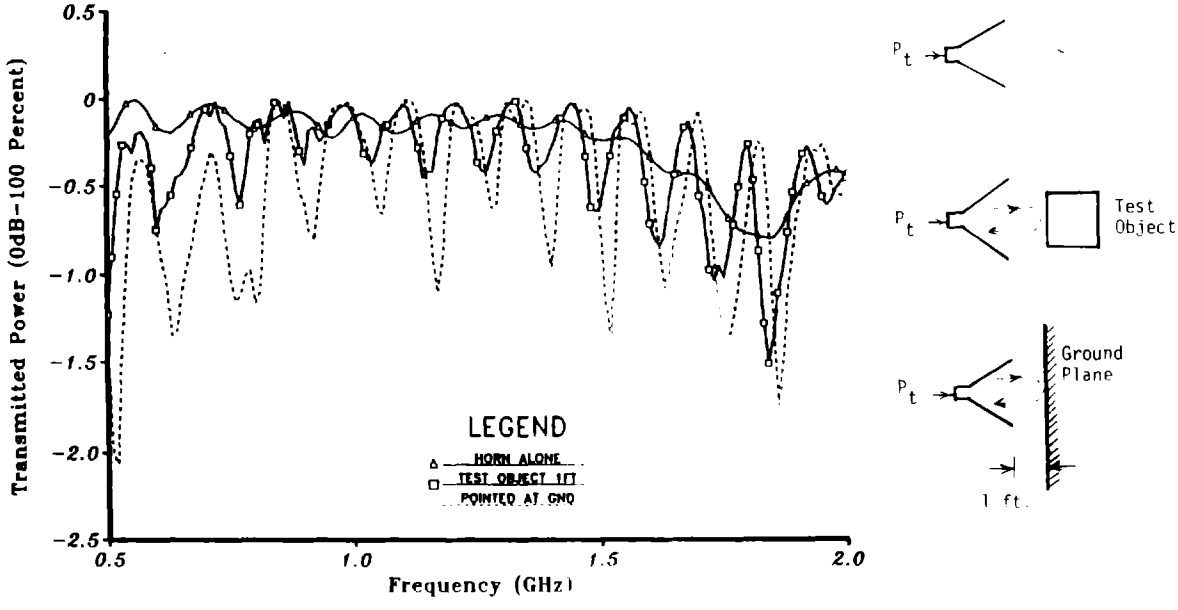

Fig. 2.10. Fractional power transmitted into the EMCO 3106 horn antenna for the three cases shown on the right.

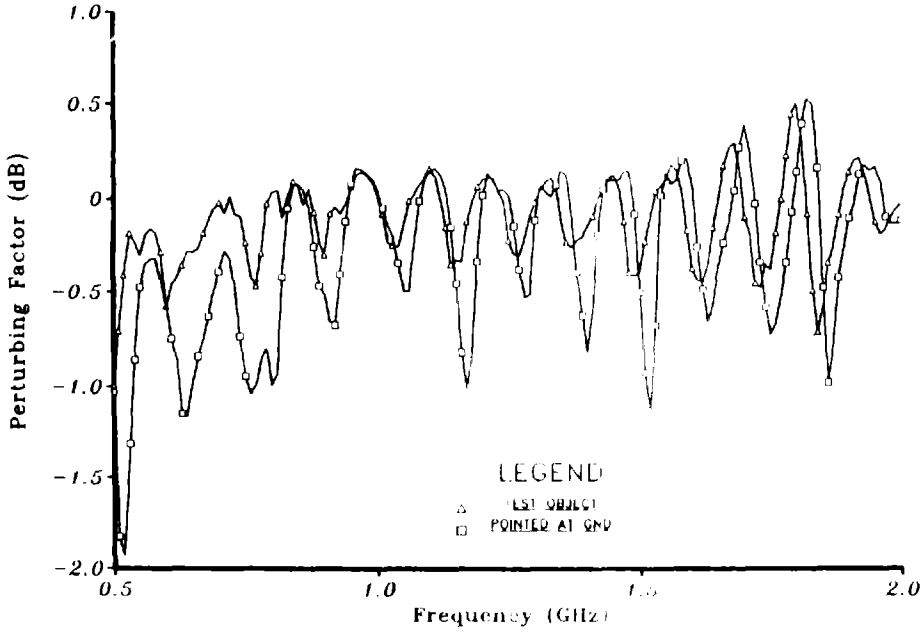

Fig. 2.11. Perturbing effect of placing the test object or a metal ground plane one foot in front of the horn aperture. Zero dB corresponds to no obstruction.

3. Description of the Test Object

The generic object used in the subsequent near-field coupling studies is shown in Figs. 3.1 and 3.2. Dubbed GOOFI, this object is 2.44 m long, configured with four internal cavities separated into different lengths by three baffles which simulate bulkheads. Eight more or less randomly-sized and randomly-positioned slot apertures are located on one side of GOOFI, two per compartment. All eight slots have the same orientation such that they couple best when the incident field is polarized along the length of the object. The slot lengths and their locations relative to the object center are tabulated in Fig. 3.1.

Since one objective of this coupling study is to investigate the effects of multiple POEs on a common coupling wire or cable, two interior wires run the full length of GOOFI. In this configuration, the cavities are strongly coupled to each other via the two wires. Consequently, energy can freely pass from one end to the other at all frequencies. The baffles merely serve to establish cavity modes in each compartment, but the resonant frequencies of these modes can propagate throughout the object by means of the common coupling wires.

The ends of both wires terminate in SMA feed-through connectors, designated as test points (TP) 1-4, as shown in Fig. 3.1. Using an automatic vector network analyzer (HP8510), the coupled voltages $V_L(f)$ could be measured at any one of the four test points. In carrying out these measurements, it was found that coupling to the two wires was very similar, which comes as no surprise. Consequently, attention focused on only the center wire, and measurements were generally restricted to TP1 and TP3.

When coupling measurements were being made at a given test point, all other test points were terminated in 50 Ω. It should be noted, however, that the use of such terminations does not guarantee an impedance match to the coupling wire, since the impedance of the wire itself is not 50 Ω. In fact, the resistive as well as the reactive components of the input impedance at any test point varies widely with frequency because of wire and cavity resonances. Thus, the use of 50 Ω terminations at unused test points was merely convenient. Similar results would be obtained if short or open circuit terminations are used.

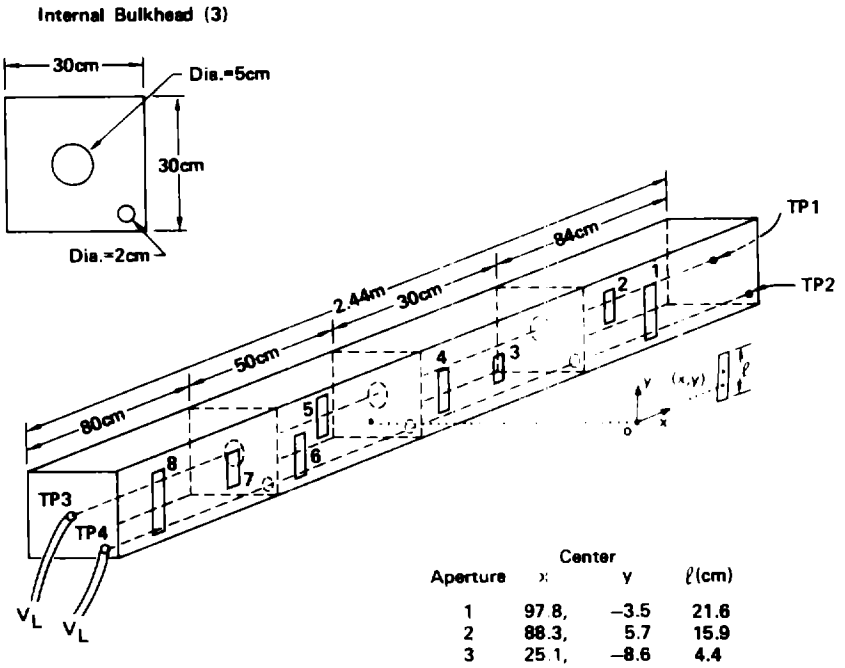

Aperture	Center x	Center y	ℓ(cm)
1	97.8,	−3.5	21.6
2	88.3,	5.7	15.9
3	25.1,	−8.6	4.4
4	14.9,	−7.6	9.8
5	−24.4,	5.7	13.0
6	−37.1,	−4.4	14.9
7	−52.7,	−3.5	12.4
8	−114.3,	−2.2	22.9

Fig. 3.1. Detailed prospective of the empty GOOFI test object.

This generic object represents what is probably a worst case in that all POEs are located on one side and respond best to the same polarization. Further, the internal compartments are strongly coupled by means of the two wires which pass end-to-end. In a more realistic object, e.g., a missile or aircraft, it is likely that the POEs would be distributed around the object and that they would each respond to different polarizations at different angles of incidence. It would be expected, therefore, that only one or two POEs on a real piece of hardware would significantly respond to a given polarization, frequency and object orientation (or incidence direction). It will be seen that the learning experiences gained from these studies give substantial insight into the how the object should be tested and the results interpreted when exposed to the near-field of a source.

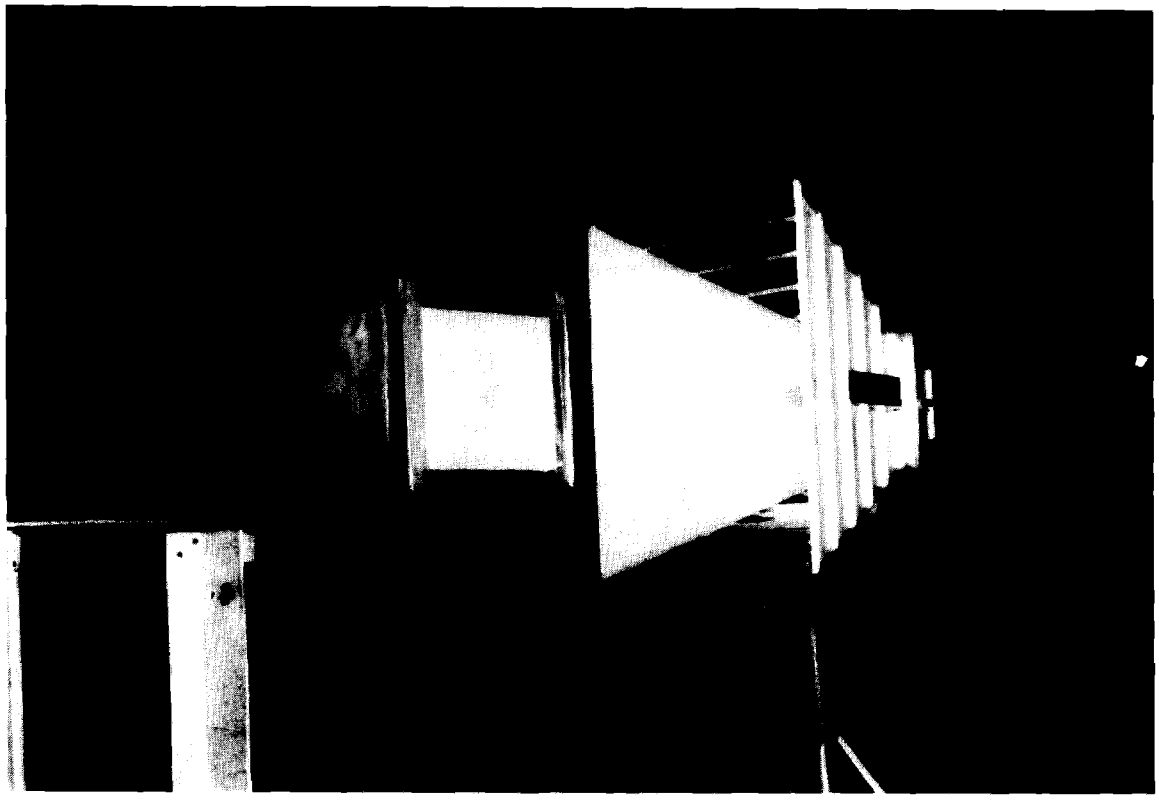

Fig. 3.2. Photograph of GOOFI being illuminated by the near-field of the horn antenna.

Fig. 3.2 shows GOOFI being illuminated by the near-field of the EMCO 3106 horn antenna in the LLNL Microwave Anechoic Chamber Facility. In evaluating the relative contributions of certain open POEs, other POE's were closed by covering them with adhesive-backed copper foil. This method of closing off unused POEs afforded 30-35 dB of shielding. This is more than adequate to accurately observe the effects of the remaining open POEs.

In addition, the separation distances between the horn aperture and the GOOFI test object were varied. Fig. 3.3 qualitatively depicts the resulting variations of the illuminating near-field 3 dB spot sizes, corresponding to the indicated separation distances. Generally, the larger spot size corresponds to the higher frequencies (2 GHz maximum), and the smaller sizes correspond to the lower frequencies (.5 GHz minimum; see Figs. 2.8 and 2.9).

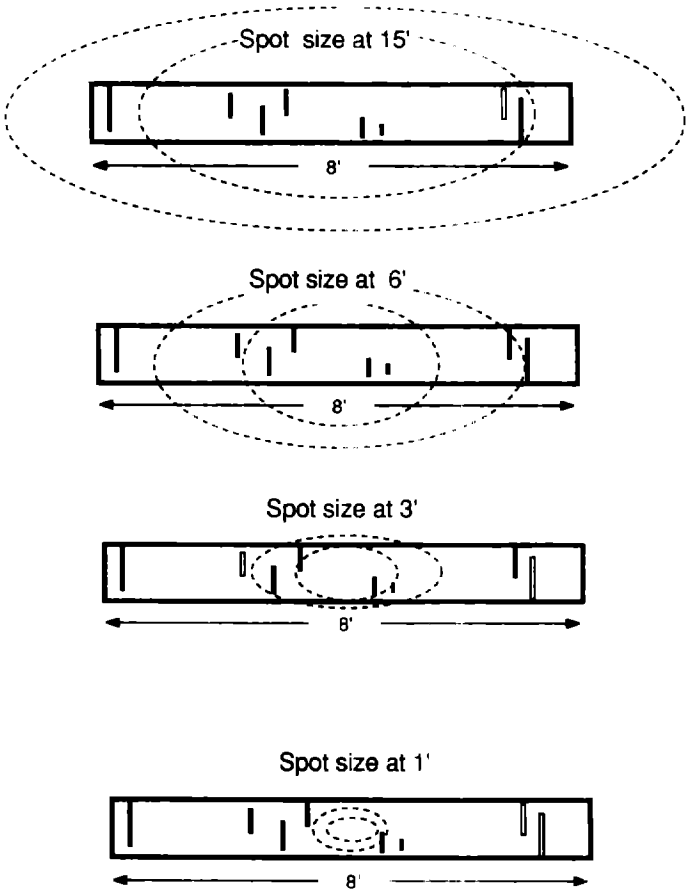

Fig. 3.3. Qualitative maximum and minimum sizes of the 3 dB contours superimposed on the GOOFI test object, corresponding to the indicated separation distances between the horn aperture and GOOFI.

Near-field coupling characterization of the empty GOOFI (Fig. 3.1) were done first. Subsequently, the four compartments inside GOOFI were partially filled with scrap hardware consisting of various pieces of electronics, dielectrics, wires, cables and microwave absorbing materials (see Fig. 3.4). The hardware was held fixed by means of expanding epoxy potting compound. Otherwise, the configuration of GOOFI remained the same as depicted in Fig. 3.1. Filling GOOFI in this manner was done in order to simulate coupling into a more realistic test object containing real electronic hardware.

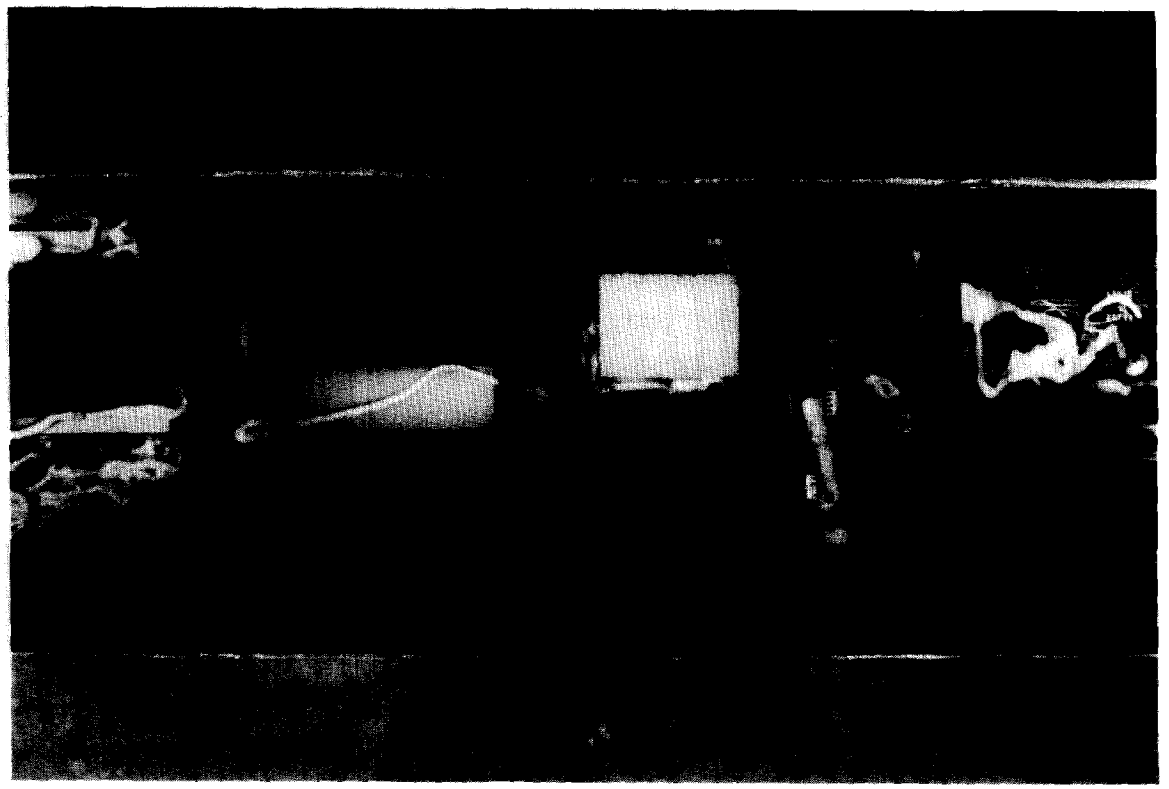

Fig. 3.4. Photograph of the GOOFI test object when partially filled with scrap electronic hardware.

4. Coupling Results

4.1 Coupling via a single POE

We first consider how well the receiving cross sections as measured when the object is in the source near-field compares with these when the object is in the source far-field. Fig. 4.1 gives such a comparison for coupling to TP1 of GOOFI via the single open POE 1 which is closest to TP1 when the object is filled with electronic hardware. Fig. 4.2 compares the near- and far-field coupling to TP1 via POE 5 which is near the middle of the filled GOOFI and removed from TP1 by two bulkheads. While filling the object obviously effects the coupling level and the detailed structure of the coupling response, it has little to do with the deviation between the near- and far-field results. A sampling of the data for the unfilled object is given in Fig. 4.3 which shows coupling via POE 4 which is removed from TP1 by one bulkhead (see Fig. 3.1). In these experiments, all other POEs were closed with adhesive-backed copper foil.

The aperture resonances are clearly evident in Figs. 4.1 and 4.2 for POEs 1 and 5, corresponding to when their lengths are nearly $\lambda_o/2$, i.e., at .69 and 1.15 GHz respectively, corresponding to the aperture lengths shown in Fig. 3.1.

In these and all subsequent data, the receiving cross section was calculated using (1) which can be expressed as

$$\sigma_{(f)} = \frac{P_L(f)}{S_{inc}(f)} = \frac{\eta_o}{R_L} \left| \frac{V_L(f)}{E_{inc}(f)} \right|^2 \qquad (5)$$

where $\eta_o = 120\pi$ and V_L is the voltage at the test point as measured by the network analyzer having an input impedance of $R_L = 50\Omega$. The magnitude ratio in (5) is readily identified as that of the antenna receiving factor of the test object, similar to (3) for the source antenna. Here S_{inc} is assumed to be given by Eq. (2) where E_{inc} is the incident electric field as measured by a calibrated receiver on boresight of the source horn in the absence of the object. As noted earlier, it is unclear what S_{inc} should be in the near-field case; here we simply took it to be Eq. (2) for a given distance from the source aperture. Strictly speaking, Eq. (2) is only appropriate for the far-field case.

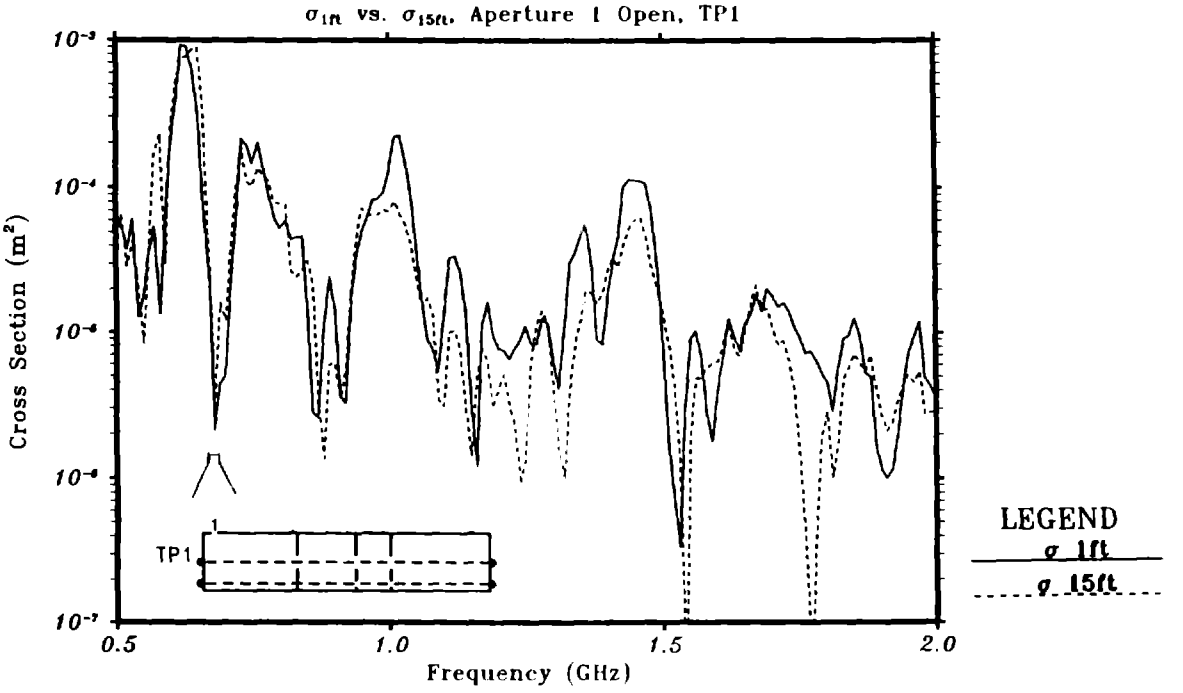

Fig. 4.1. Comparison of near- and far-field receiving cross sections for coupling via POE 1 which is closest to TP1. Object filled.

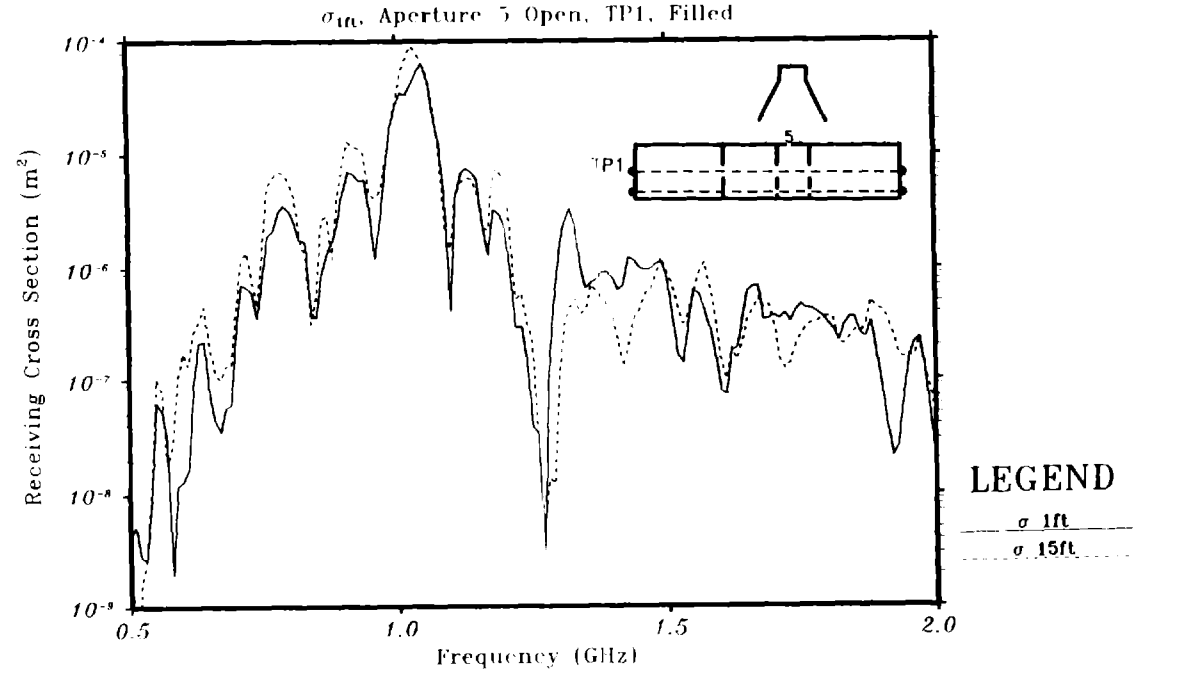

Fig. 4.2. Comparison of near- and far-field receiving cross sections for coupling to TP1 via POE 5 which is near the middle of the test object. Object filled.

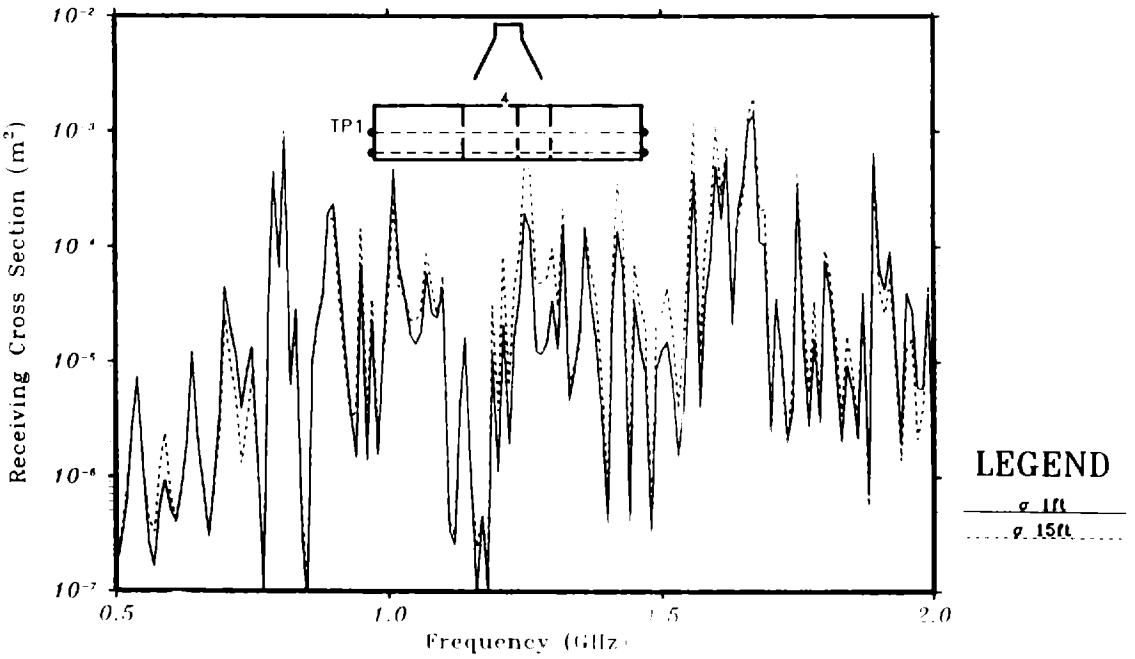

Fig. 4.3. Comparison of near- and far-field receiving cross sections for coupling to TP1 via POE 4 which is near the middle of the test object. Object empty.

In spite of these assumptions, the near-field receiving cross section (when the aperture is at 1 ft. from the source aperture) captures the main features of the far-field cross section (when the aperture is 15 ft. from the source aperture). A few of the details are not replicated, but the trend and overall level are reproduced rather well. This suggests that Eq. (2) is a reasonably good approximation to S_{inc} in the source near-field.

An important utility of this observation is that a good approximation to the far-field receiving cross section of a single POE can be achieved by placing the object in the source near-field, provided that the POE is uniformly illuminated.

4.2 Coupling via multiple POEs

When coupling via multiple POEs, the same applies provided that the illuminated area on the object contains the POEs which significantly contribute. Obviously, if one or two strongly contributing POEs are not properly illuminated when the source is near the object, the near- and far-field receiving cross sections will differ substantially. This is obvious for the intensity of the incident field, because the coupled intensity is in direct

proportion to the incident intensity. But the phase of the incident field is another matter; it will be dealt with shortly. Whether all of the important POEs on the object exterior are properly illuminated is referred to as the "spot size" problem.

Two POEs (4 and 5) were open simultaneously in the data of Fig. 4.4 (empty object). From Fig. 3.1 it is seen these two POEs are 39.3 cm apart. Consequently, when the source is centered between them at 1 ft. (30.5 cm) from the object, both POEs are illuminated nearly equally. Subsequent tests showed that 4 and 5 contribute 5.5 and 17% respectively, to the total accumulated energy, relative to the summed individual contributions of all eight apertures (see table 2). But it was also found that they do so at different frequencies. As a result, it is not surprising that their reviewing cross sections add to give very good comparison with the measured far-field (15 ft.) receiving cross section in Fig. 4.4. Almost all of the structural detail is captured in the near-field case, compared to the far-field case.

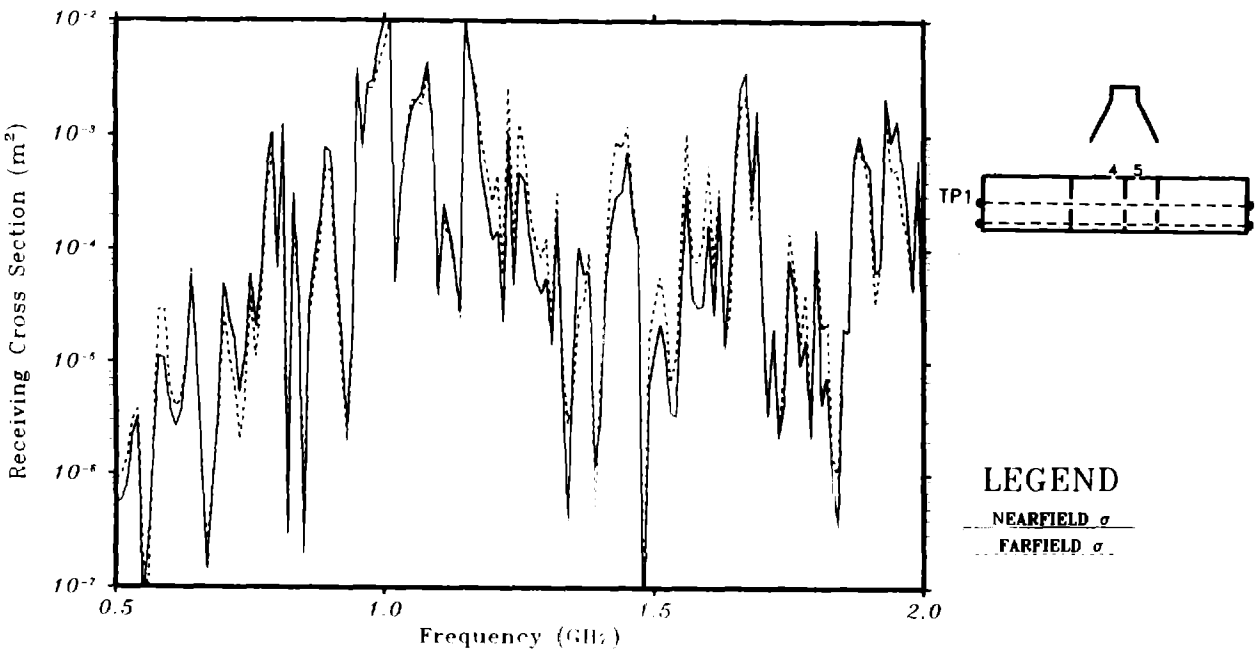

Fig. 4.4. Comparison of near- and far-field receiving cross sections when POEs 4 and 5 are illuminated simultaneously. Empty object.

This situation becomes somewhat more complex when two or more POEs contribute simultaneously. Such is the case in the data sets of Figs. 4.5 and 6, and 4.7 and 8, corresponding to when the object is empty and filled with electronic hardware, respectively. The upper figures show the relative individual contributions, σ_n, of the eight POEs when each is excited separately in the near-field (source is 1 ft from each POE) and the other POEs are closed. Each of these σ_ns are compared to the true (or total) receiving cross section σ_t as measured when the object is in the far-field (15 ft.) and all eight apertures are open simultaneously. These data are smoothed 11% to show the trends rather than the fine details.

The lower figure of each set compares the true $(\sigma_t)_{15\ ft.}$ and the incoherent scalar sum of all of the σ_ns, i.e.,

$$\sum_{n=1}^{8} (\sigma_n)_{1\ ft.} \tag{6}$$

Both sets of data were taken at TP1; the results at TP3 were similar and hence not given here.

In the upper Figs. 4.5 and 4.7 it is seen that there are frequency ranges where only one POE clearly dominates, while two or more POEs may contribute significantly over other frequency ranges. Based on the conclusions of the preceding section, it can be argued that at any frequency where only one POE clearly dominates the near-field, σ_n of that POE should correspond well with σ_t. For example, in Fig. 4.7, σ_1, which clearly dominates below about 0.8 GHz, replicates the true $(\sigma_t)_{15\ ft.}$ rather well. However, at about 0.9 HBz, σ_1, σ_2, and σ_6 become comparable to each other (Fig. 4.7). Since the true $(\sigma_t)_{15\ ft.}$ is actually the result of squaring the phasor sum of voltages due to all of the individual POE contributions, it is very likely that at a few frequencies these contributions can add destructively. Such is clearly the situation at 0.9 GHz in Fig. 4.8, for example. Similar interferences are exhibited in σ_t at 1.0, 1.15, 1.4 and 1.8 GHz. Because of the mathematical fact that

$$\Sigma|V_n|^2 \geq |\Sigma V_n|^2 \tag{7}$$

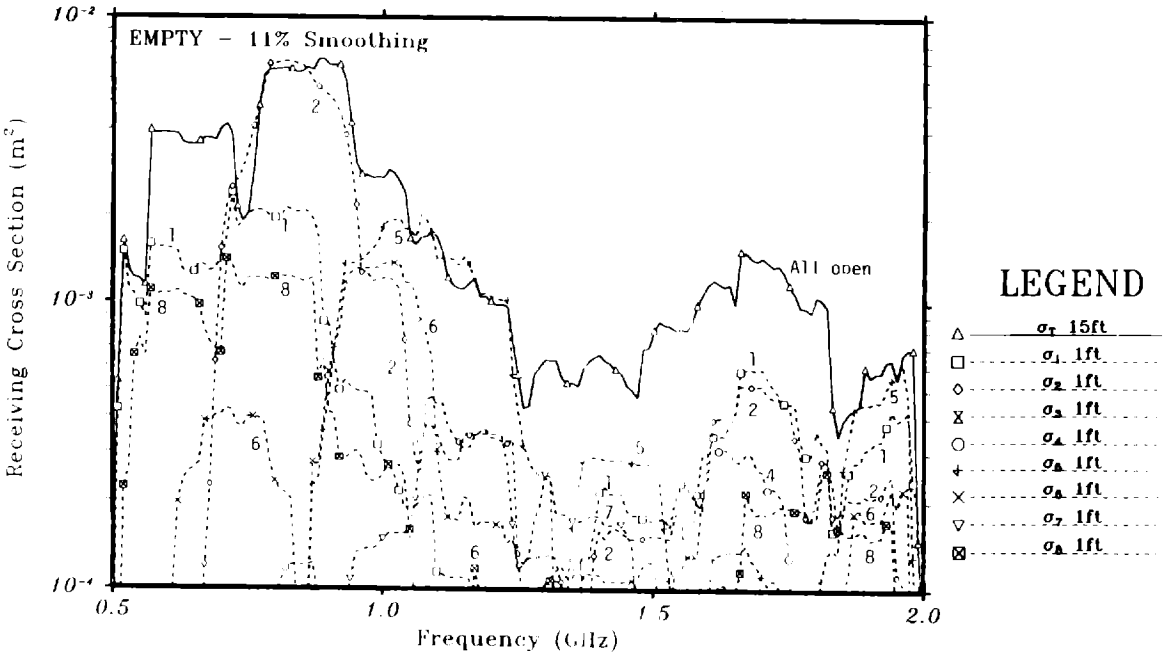

Fig. 4.5. Relative contributions of the eight POEs when excited separately in the near-field, and the total σ_t when all POEs are excited simultaneously in the source far-field. Object empty. TP1

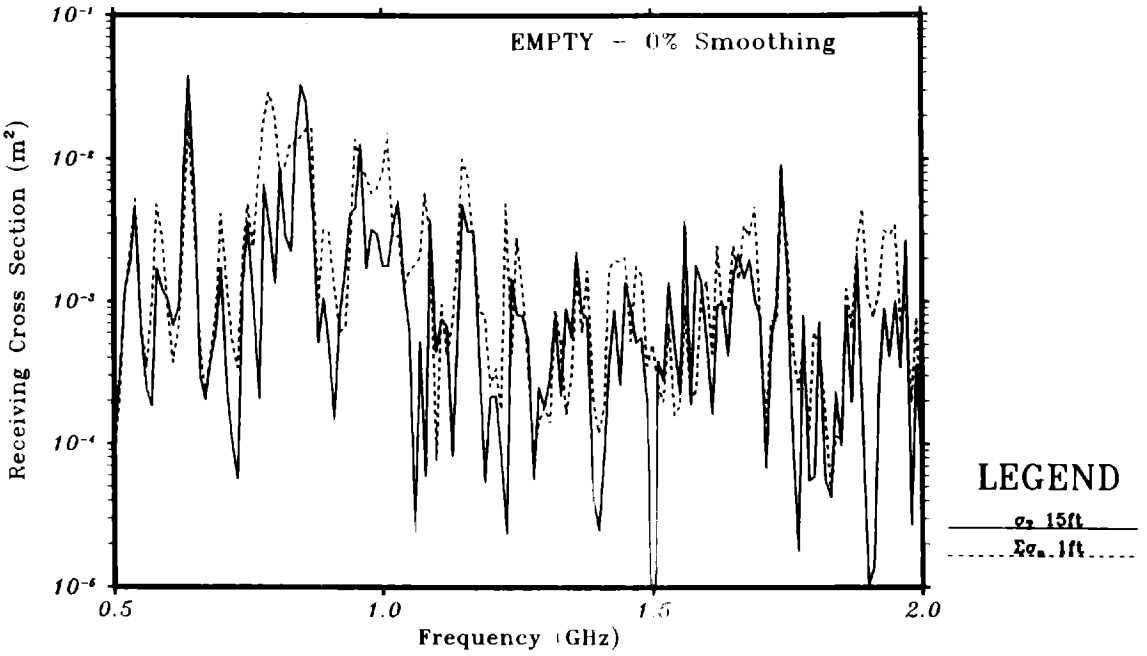

Fig. 4.6. Comparison of cumulative contributions when all eight POEs are excited simultaneously in the source far-field $(\sigma_t)_{15\ ft.}$, and the cumulative incoherent near-field contributions of the individual POEs $(\Sigma\sigma_n)_{1\ ft.}$ Object empty. TP1.

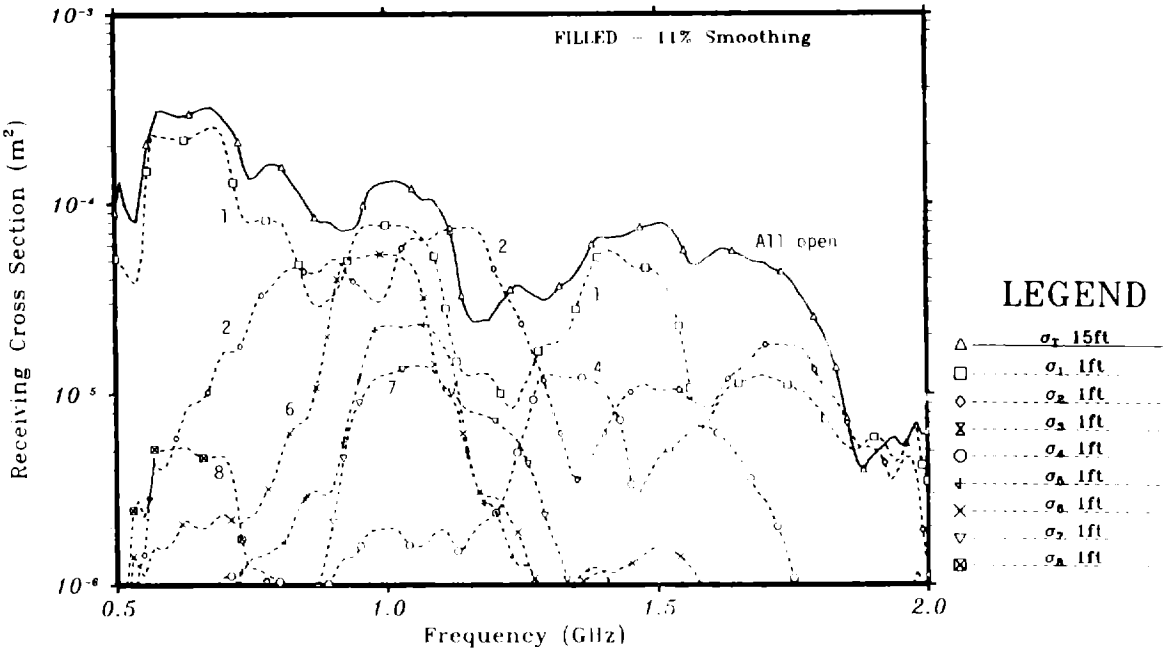

Fig. 4.7. Relative contributions of the eight POEs when excited separately in the near-field, and the total σ_t when all POEs are excited simultaneously in the source far-field. Object filled. TP1.

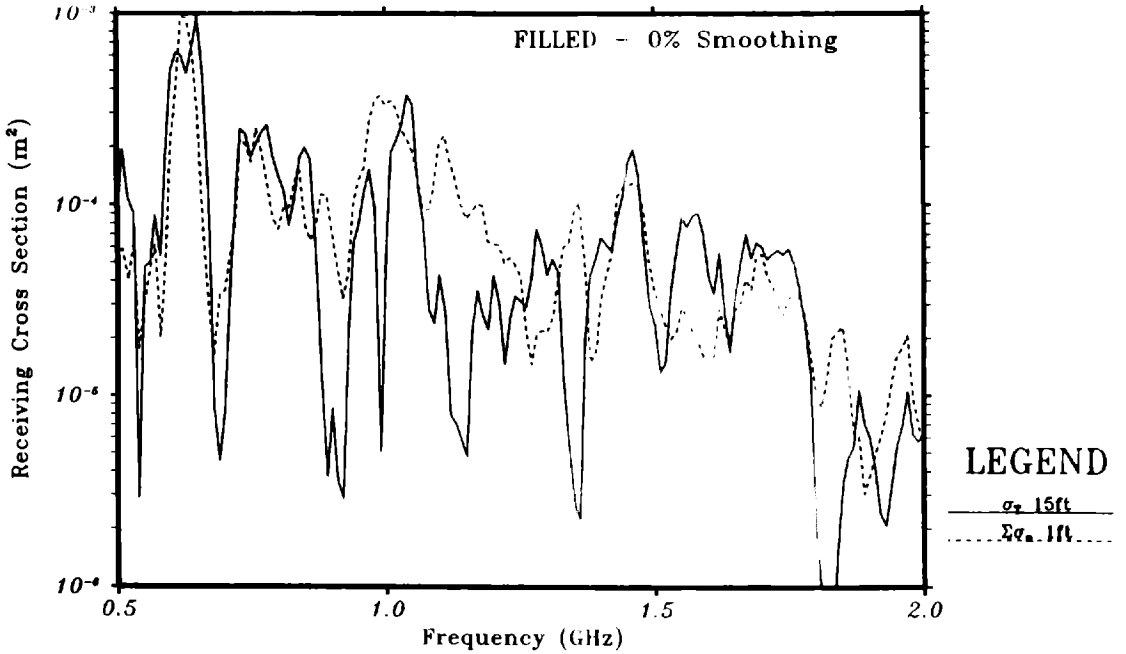

Fig. 4.8. Comparison of cumulative contributions when all eight POEs are excited simultaneously in the source far-field $(\sigma_t)_{15\ ft.}$, and the incoherent cumulative near-field contributions of the individual POEs $(\Sigma\sigma_n)_{1\ ft.}$ Object filled. TP1.

(i.e., the scalar sum equals or exceeds the magnitude of the phasor sum), where $V_n = |V_n|e^{j\Phi_n}$ is the complex voltage phasor contribution of each POE $\Sigma\sigma_n$ is expected to overestimate σ_t. Recall Eq. (5) which defines σ_n as proportional to $|V_n|^2$. This is clearly the case in both Figs. 4.6 and 4.8, where it is seen that $(\Sigma\sigma_n)_{1\text{ ft.}}$ overestimates $(\sigma_t)_{15\text{ ft.}}$ over the majority of frequencies. Since $(\Sigma\sigma_n)_{1\text{ ft.}}$ and $(\sigma_t)_{15\text{ ft.}}$ are calculated from different experiments which generate different data sets, there are a few frequencies where σ_t exceeds $\Sigma\sigma_n$ as might be expected.

To gain further insight into the degree of overestimation, Figs. 4.9 and 4.10 show the ratios

$$\frac{\left(\sum_{n=1}^{8}\sigma_n\right)_{1\text{ ft}}}{(\sigma_{\text{total}})_{15\text{ ft.}}} \tag{8}$$

corresponding to the the empty and filled data of Figs. 4.6 and 4.8 respectively. Here, any overestimation of $\Sigma\sigma_n$ compared to σ_t is above the zero dB line. While smoothing these data (11% in this case) shows the trend vs. frequency, it is also of interest to compute the proportion of all frequencies[1] where $(\Sigma\sigma_n)_{1\text{ ft.}}$ exceeds $(\sigma_t)_{15\text{ ft.}}$ as shown in Fig. 4.11. For example, for 50% of all frequencies, $\Sigma\sigma_n$ exceeds σ_t by .5 dB and 2 dB in the filled and empty cases respectively. Similarly, for only 10% of all frequencies in the .5 → 2 GHz range, $\Sigma\sigma_n$ exceeds σ_t by 10 dB (filled) and 8 dB (empty). In these data, the average and the RMS deviation values are 2.9 and 5.74 dB for the empty object, and 1.54 and 5.4 dB for the filled object, respectively.

But in spite of these errors, which are the result of incoherent or scalar addition rather than coherent or phasor addition, when two or more POEs are contributing, the overall trend of $(\Sigma\sigma_n)_{1\text{ ft.}}$ is remarkably similar to that of $(\sigma_t)_{15\text{ ft.}}$ in both the filled and unfilled cases. It can therefore be said that the incoherent sum $(\Sigma\sigma_n)$ for multiple POEs as measured separately in the near-field will, in general, overestimate the coherent trend of

[1]As the processes involved here have a sometimes strong deterministic (in contrast to random) nature, we resist the temptation to use such terms as "probability," "mean," and "standard deviation," etc. Instead, we use the analogous terms "proportion of frequencies," "average," and "RMS deviation" in order to preserve the deterministic flavor.

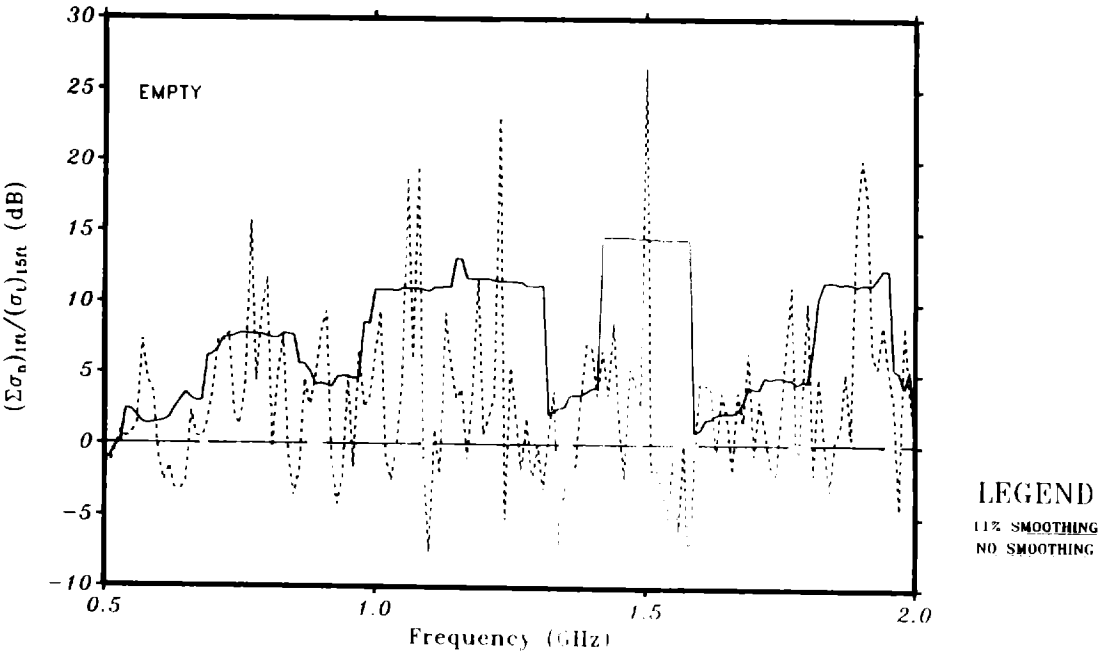

Fig. 4.9. Ratio of $\Sigma\sigma_n/\sigma_t$ corresponding to the data in Fig. 4.6. These data show the degree to which $(\Sigma\sigma_n)_{1\text{ ft.}}$ overestimates the true $(\sigma_t)_{15\text{ ft.}}$ Object empty. TP1.

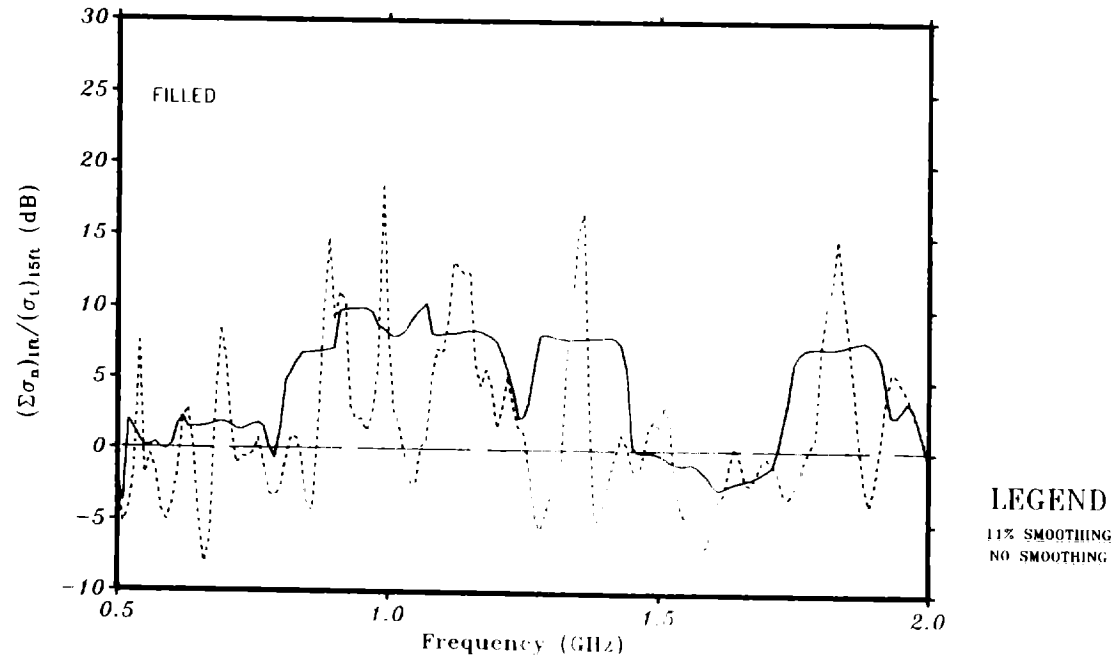

Fig. 4.10. Ratio of $\Sigma\sigma_n/\sigma_t$ corresponding to the data in Fig. 4.8. These data show the degree to which $(\Sigma\sigma_n)_{1\text{ ft.}}$ overestimates $(\sigma_t)_{15\text{ ft.}}$ Object filled. TP1.

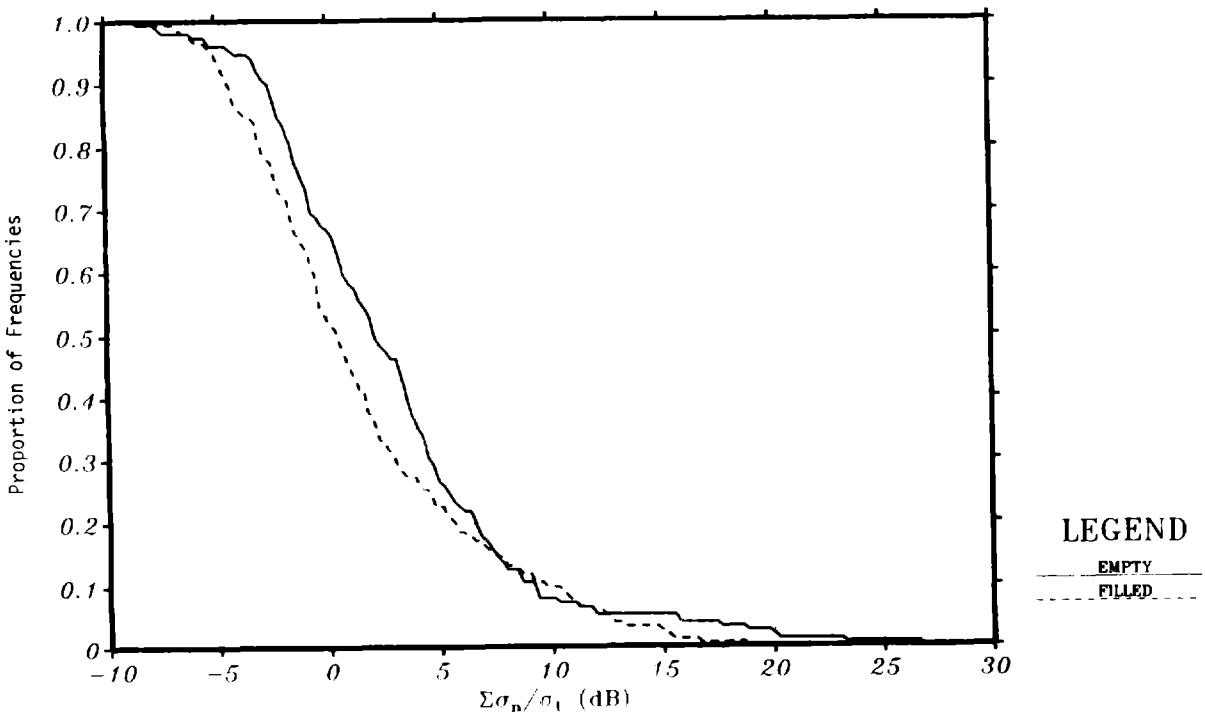

Fig. 4.11. Proportion of frequencies for which $(\Sigma\sigma_n)_{1\ ft.}$ exceeds $(\sigma_t)_{15\ ft.}$ corresponding to the data in Figs. 4.5 and 4.7.

the true far-field receiving cross section, σ_t. Furthermore, it does not replicate the finer details vs. frequency except when only one POE, σ_n, dominates.

The reason why the incoherent sum $\Sigma\sigma_n$ tends to replicate the coupling stems from the fact that the phases of the coupled signals, relative to each other, are rapidly changing as the frequency varies. In turn, these rapidly changing phases are a consequence of multiple cavity and coupling cable modes and resonances, complex coupling from cavity-to-cavity and complex scattering by the interior bulkheads and hardware. These matters are discussed further in the following subsection 4.3.

In passing, note that all the POEs tend to contribute at the higher frequencies when the object is empty (Fig. 4.5). Such is not the case when it is filled (Fig. 4.7) because of increased internal losses. It is also apparent that the level and the degree of structural detail is much greater when the object is empty (Figs. 4.5 and 4.8) than when it is filled with hardware (Fig. 4.7 and 4.9). Section 4.5 discusses these features in greater detail.

Finally, these data emphasize what is probably obvious: when testing with an HPM near-field source at a chosen frequency, low level characterization is essential in order to determine how the individual POEs couple, i.e., which POEs are important and over what frequencies, angle of incidence and polarization they are important. Armed with this information, informed decisions can be made regarding how the object should be tested for HPM susceptibility.

4.3 Further discussion on deterministic and stochastic coupling

The signal traveling from a given POE to a given terminal does so over many more or less random coupling paths as the frequency, angle of incidence, or the polarization of the incident field changes. This is due to the manner in which the many cavity and cable resonance modes are excited, as well as many other factors such as cavity-to-cavity coupling. Further, in the case of coupling to a susceptible component pin, circuit trace and component resonances make the coupling path even more random-like, i.e., stochastic. Consequently, as the frequency changes, the phase as well as the amplitude of a signal arriving at a given terminal or pin via a given POE is likely to be a more or less stochastic process. Furthermore, the contribution of a given POE relative to other possibly contributing POEs may also be a stochastic process.

But the problem is also deterministic. Consequently, the total voltage (or current) at a given terminal or pin at a given frequency is actually a coherent sum of complex phasors, as depicted in Fig. 4.12. Here, $V_n \left(= | V_n | e^{j\phi_n}\right)$ is the complex phasor representing the contribution of the nth POE at a given frequency. As the frequency changes, one can imagine each $| V_n |$ and ϕ_n as rapidly changing, leading to the stochastic property described above.

With this picture in mind, one might ask how the true or coherent sum compares with incoherent sums (i.e., dealing only with voltage magnitudes $| V_n |$, without accounting for phase, ϕ_n). Since we are concerned with power delivered to the terminal or pin, we consider three cases.

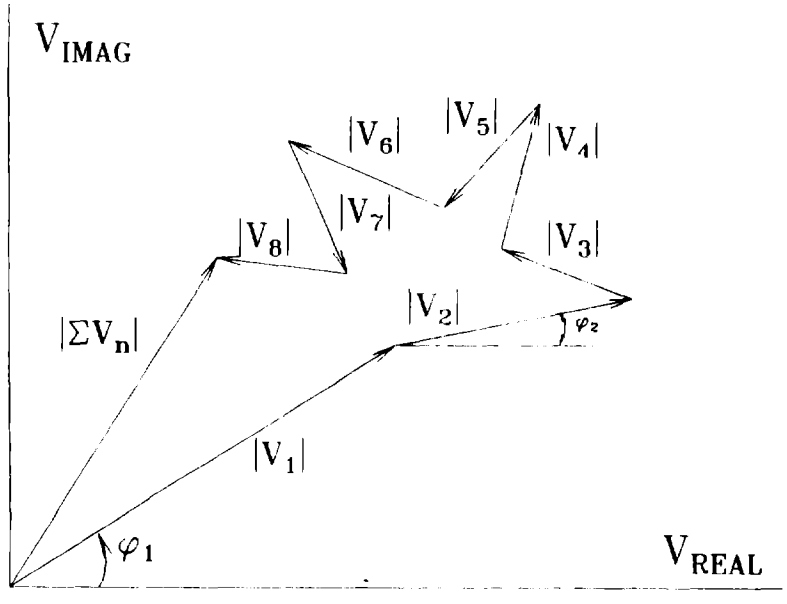

Fig. 4.12. Construction of a phasor sum, $|\Sigma V_n|$ for random $V_n = |V_n| e^{j\phi_n}$

{1} The coherent sum, $(|\Sigma V_n|)^2$ which results from adding the complex phasors, and squaring the magnitude of this sum. When normalized by $|E_{inc}|^2$ and multiplied by the impedance ratio η_o/R_L, this sum should reproduce the true receiving cross section, σ_t, under ideal conditions to be discussed shortly.

{2} The incoherent sum, $(\Sigma |V_n|^2)$. When normalized by $|E_{inc}|^2$ and multiplied by η_o/R_L, this sum is equivalent to $\Sigma\sigma_n$ in the previous subsection 4.2. As already seen, this type of incoherent sum tends to overestimate σ_t, and does not capture all of the possible destructive features of σ_t.

{3} The incoherent sum, $(\Sigma |V_n|)^2$. When normalized by $|E_{inc}|^2$ and multiplied by η_o/R_L, this represents an upper bound to σ_t which might occur in the extremely unlikely event that all the V_ns add in phase at all frequencies.

To test these three approximations, several experiments were conducted. First, GOOFI was illuminated in the far-field (15 ft.) of the source antenna with all eight POEs open simultaneously. This determined the true receiving cross section, σ_t, to which the three cases discussed above are compared. Then, with the object at the same far-field position, the complex phasor voltage contributions of each of the eight POEs were separately measured, all the other POEs being closed with adhesive-backed copper foil.

First consider the coherent sum $(|\Sigma V_n|)^2$ as defined by {1} above. In order to compute this phasor sum three assumptions are necessary:

(a) That the phase of the incident field (with respect to the reference voltage being supplied to the network analyzer measuring instrument) is stable at each frequency. This stability must be maintained over the difference in the long phase paths between the reference signal and the signal being measured by the network analyzer during the time that it takes to separately measure all eight POEs. This degree of phase stability is only possible using a frequency synthesized source.

(b) That mutual coupling between POEs is negligible. If such is not the case, altering the mutual coupling between open POEs may alter any one or more of the phasor contributions V_n at the given terminal or pin.

(c) That physical movement of the object (exterior movement or changes in the interior configuration) during the process of opening and closing the eight POEs does not alter the coupling. Of course, altering the POEs themselves does alter the coupling (which is the object of the experiment), but care must be taken to ensure that other physical changes do not also occur.

Obviously, these experiments must be carried out with great care and patience, and some inaccuracies are expected to occur, especially at the higher frequencies.

The reconstruction results of the coherent sum $(|\Sigma V_n|)^2$ as discussed under {1} above are given in Fig. 4.13, compared to the true σ_t as measured with all eight POEs open simultaneously. Considering the sources of error as explained under (a), (b) and (c) above, the two curves are in remarkable agreement. In these and subsequent data comparisons, it is understood that all of the sums $\Sigma(\ )$ were normalized by $|E_{inc}|^2$ and

multiplied by η_o/R_L in accordance with Eq. (5), in order to make direct comparisons to the true σ_t.

The incoherent sum $\left(\Sigma \mid V_n \mid^2\right)$ which represents the sum $\Sigma\sigma_n$ as discussed under {2} above are compared to the true σ_t in Fig. 4.14. As was seen in Sec. 4.2, this sum approximates σ_t, but does not capture the destructive details of σ_t.

The incoherent sum $\left(\mid \Sigma \; V_n \mid\right)^2$ which represents an upper bound to σ_t as discussed by {3} above is given in Fig. 4.15. Clearly, this incoherent sum overestimates σ_t over most of the frequency range. Any underestimations are likely due to mutual coupling between POEs and to any changes in the test object which may have occurred during the course of opening and closing the eight POEs.

Fig. 4.16 shows the proportion of frequencies for which $\Sigma(\;)$ exceed σ_t for these three methods of computing the sums, using the data of Figs. 4.13 thru 4.15. Here, for 50% of the frequencies, the coherent method {1} underestimates σ_t by –1 dB, the incoherent method {2} is equally below or above σ_t, and the incoherent (bounding) method {3} overestimates σ_t by 2.6 dB. The averages and RMS deviation are given in Table 1.

Table 1

Average and RMS deviations for the three summing methods, relative to the true receiving cross section, σ_t.

	Average (dB)	RMS deviation (dB)
$(\Sigma\, V_n)^2$	–.806	3.87
$\Sigma \mid V_n \mid^2$	+1.28	4.57
$\left(\Sigma \mid V_n \mid\right)^2$	+3.65	5.18

From the results of the preceding three examples, as well as those of Sec. 4.2, it is apparent that the phase of the individual contributing POEs must be properly included in order to capture all of the structural detail contained in the true coupling response. This is especially true if only a few POEs are contributing nearly equal amplitudes to the total

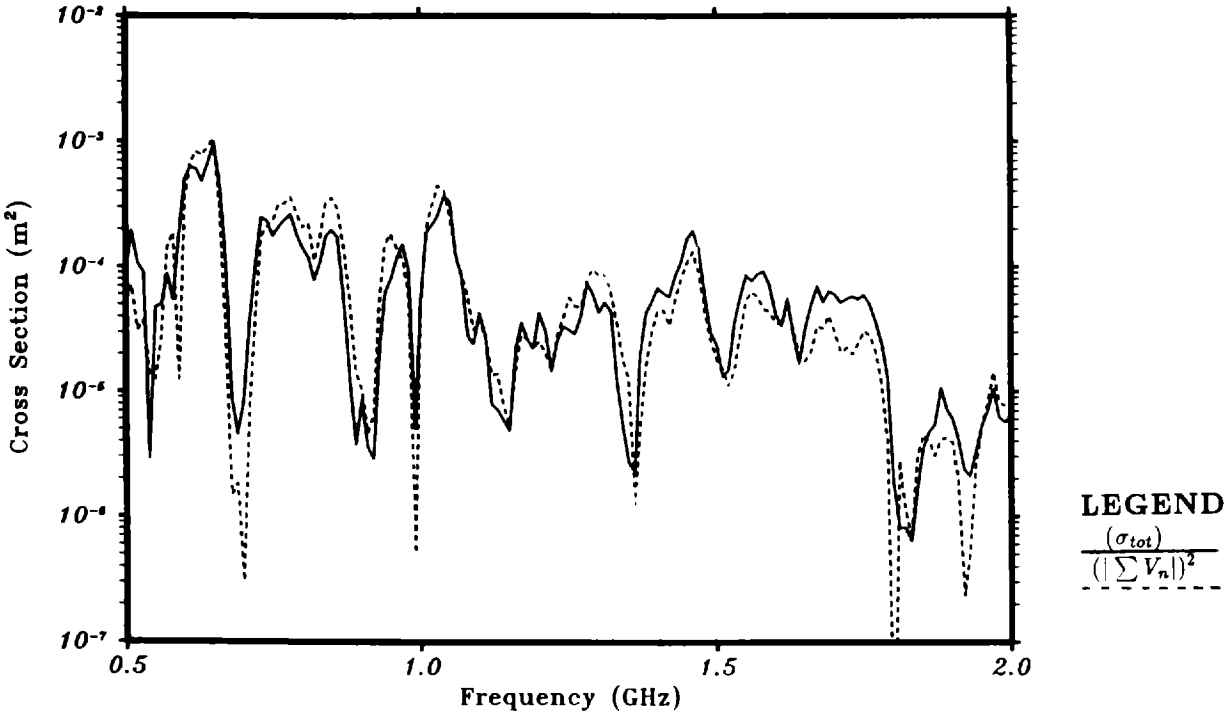

Fig. 4.13. Comparison of the true σ_t with the coherent sum $(| \Sigma V_n |)^2$.
Distance = 15 ft. Object filled. TP1.

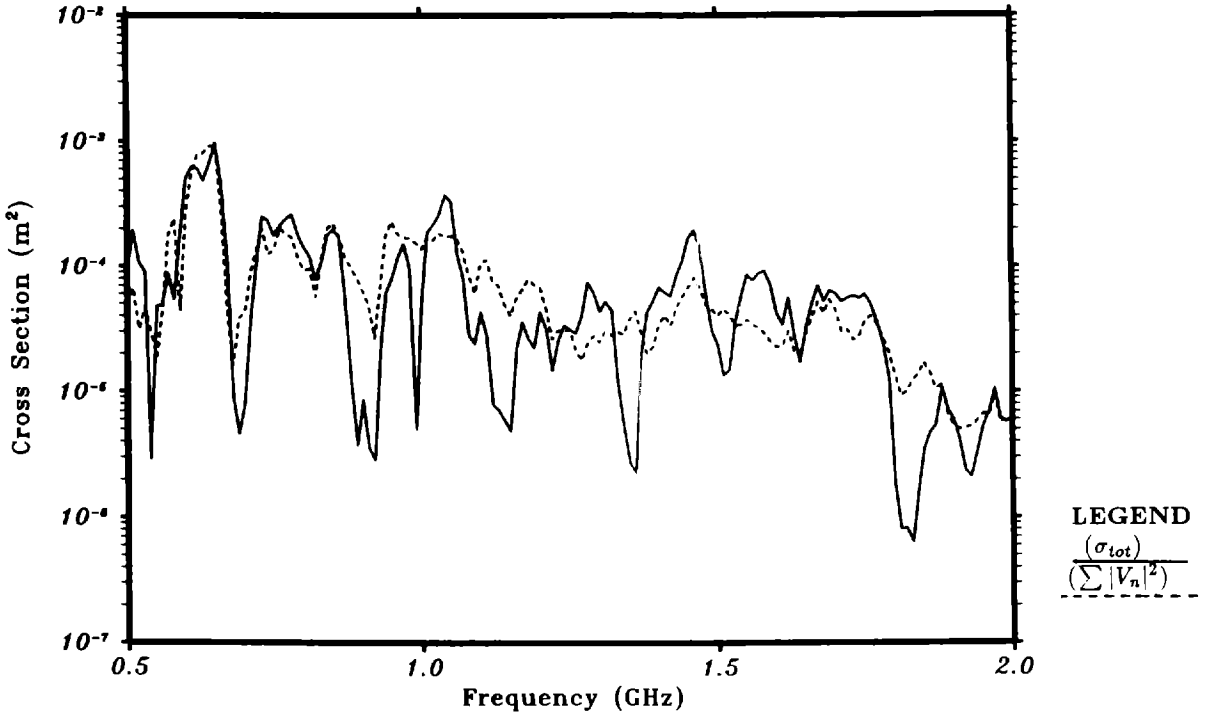

Fig. 4.14. Comparison of the true σ_t with the incoherent sum $(\Sigma | V_n |^2)$.
Distance = 15 ft. Object filled. TP1.

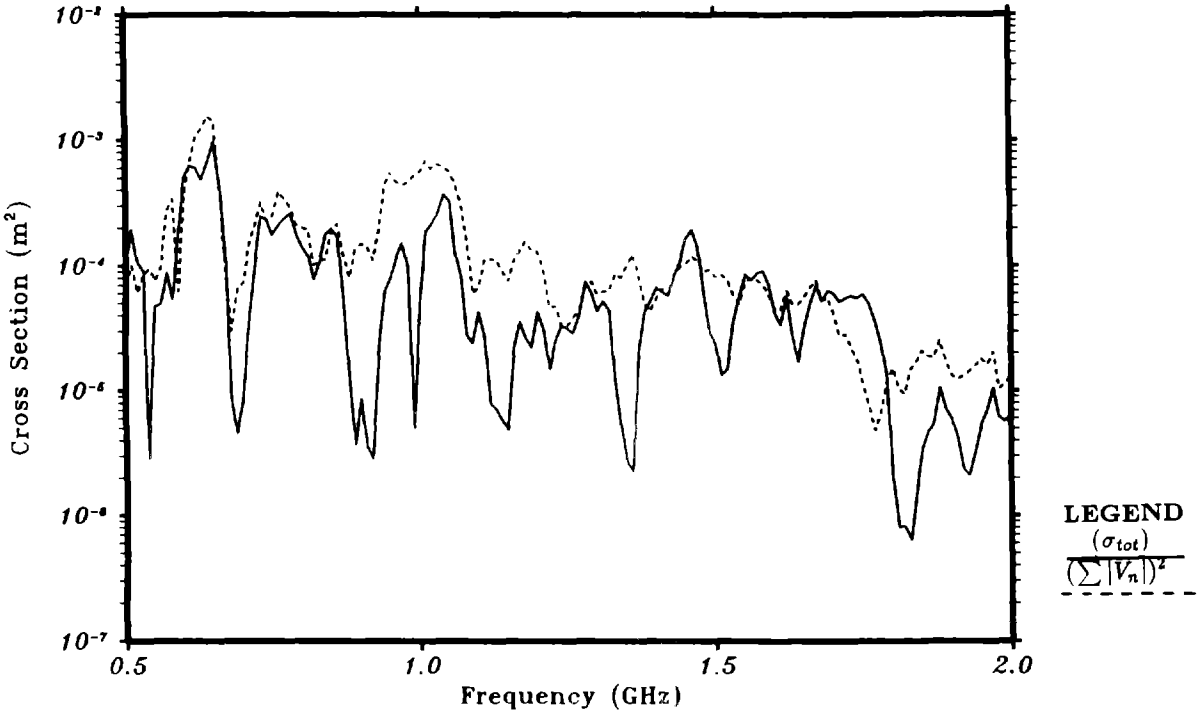

Fig. 4.15. Comparison of the true σ_t with the bounding incoherent sum $(\Sigma \mid V_n \mid)^2$. Distance = 15 ft. Object filled. TP1.

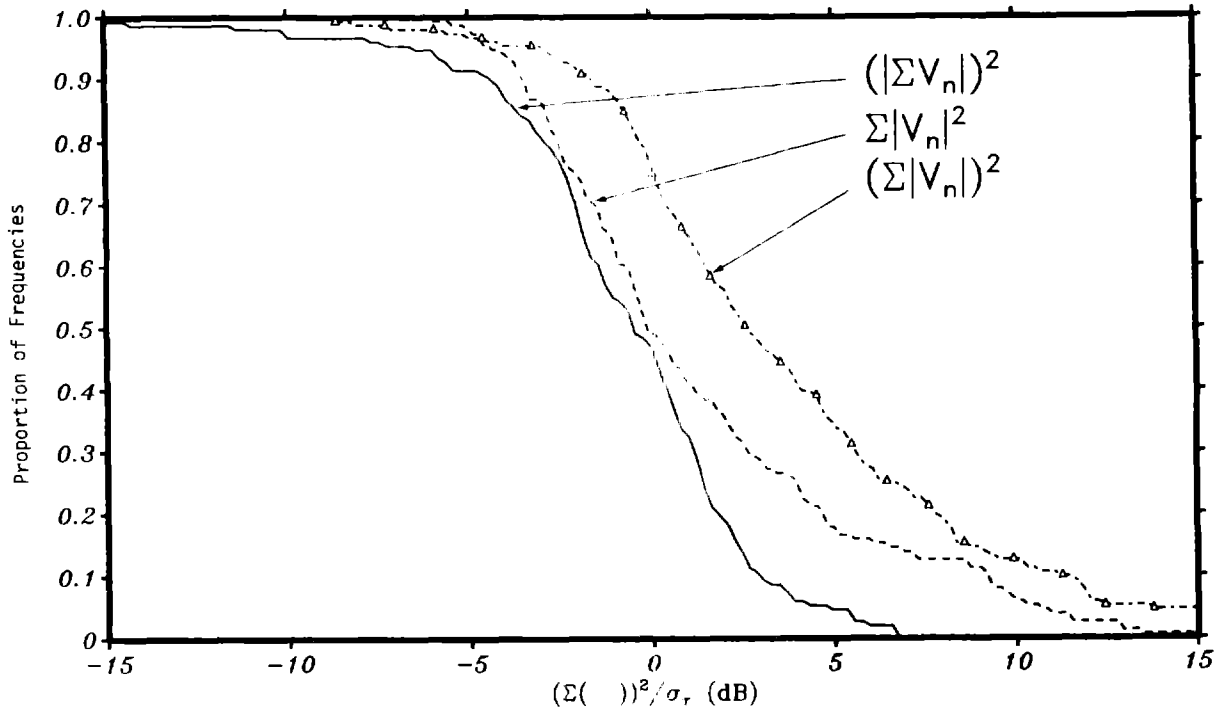

Fig. 4.16. Proportion of frequencies that $\Sigma(\ )$ exceeds the true σ_t, corresponding to the data of Figs. 4.13 - 4.15. Object filled. TP1.

signal coupled at a given frequency, angle of incidence, and polarization of the incident fields. Thus, if such detailed destructive interference data is needed to accurately assess the susceptibility of a complex system to HPM, it is necessary to illuminate the most important part of the whole system by a source which is not too close to the test object. This source must have a spot size which is sufficient to properly excite all of the important POEs simultaneously.

But if one is only concerned with the coupling trend over frequency (without replicating the exact details of destructive interference), the incoherent sum $\Sigma\sigma_n$ (as described by method {2}) is sufficient. Further, each of the individual σ_ns can be approximately measured independently by a near-field source antenna in low-power characterization tests as was shown in Sec. 4.1. This not only permits predicting the trend of the true receiving cross section, σ_t, but also yields information about which σ_ns (or POEs) are important as a function of frequency, angle of incidence and polarization. This information is very useful in deciding the necessary placement and spot size of the source antenna in actual HPM tests. Incidentally, the source antenna used to characterize the test system need not be the same one used for HPM testing.

4.4 Angular dependence

All of the preceding examples are for broadside incidence, but the conclusions still apply for other angles of incidence. Fig. 4.17 shows the invariance of the coupling via the four centermost POEs for an incidence angle of 30°. Here, the position of the source aperture was located at 1, 3, 6, and 15 ft. from the object center. For clarity, these data were smoothed 3.3% in order to remove some of the structural detail.

As was true for broadside incidence (Secs. 4.1 and 4.2) these results show that the receiving cross section is insensitive to the distance of the source antenna aperture to the excited POEs. Small deviations which are mainly in the peaks and valleys suggests that the phase (and perhaps the amplitude) distribution of the incident field is changing with source position, but these variations are apparently small. Assuming that the peaks and valleys are due to alignment of the phasors in Fig. 4.12, one can imagine that small deviations in amplitude or phase of just one of the phasors will cause the peak or valley to become blurred as in Fig. 4.17.

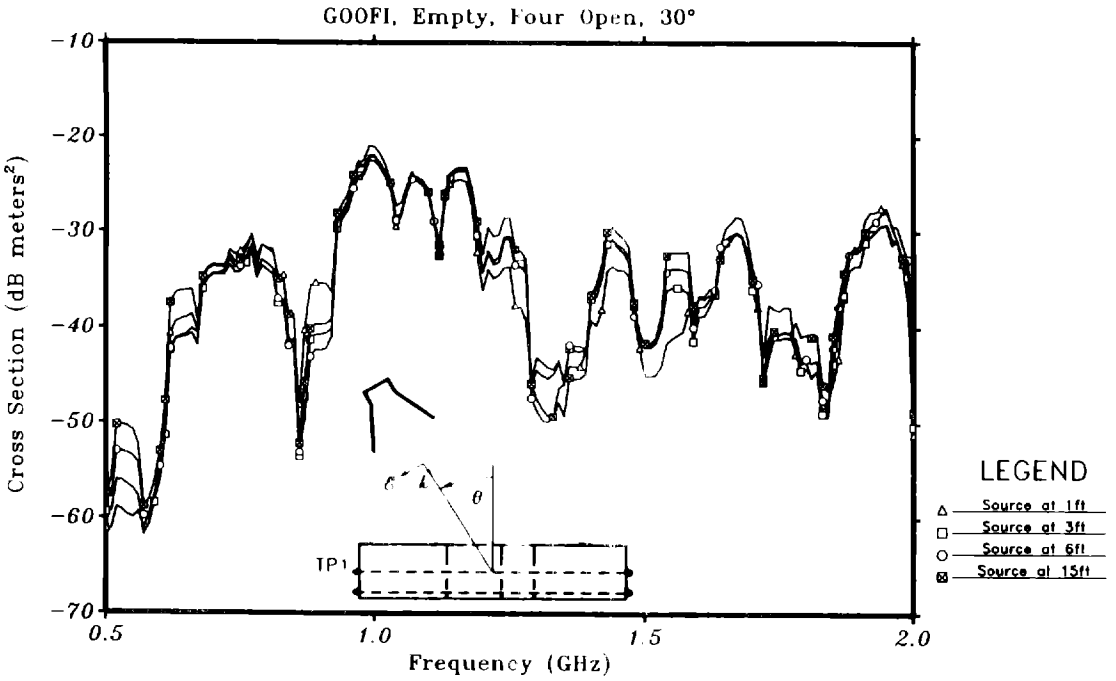

Fig. 4.17. Receiving cross-section for oblique incidence ($\theta = 30°$). The parameter is the position of the source antenna aperture from the object center. Empty. TP1.

In Figs. 4.18 and 4.19 the parameter is the angle of incidence ($\theta = 0$ and 30°). The aperture of the source antenna is fixed at 3 ft. (near-field, Fig. 4.18) and at 15 ft. (far-field, Fig. 4.19) from the test object center. We note the weak angular dependence of the trend for all frequencies, but that the change in phase of the incident field is causing obvious deviations in the receiving cross section at the peaks and valleys. Thus, variation in the phase of the incident field are altering the points where constructive and destructive interferences are occurring.

Although the test object used here (Fig 3.1) was designed to represent realistic coupling into a complex system, the preceding results have shown that its coupling via eight or fewer POEs is not totally random. Consequently, it is not particularly appropriate for demonstrating high degrees of constructive and destructive interferences which may result from phase variations between a few nearly equally contributing POEs.

To demonstrate that such features can and do occur under idealized conditions, this section concludes with an example in which the coupling has little randomness and is highly deterministic. Experiments were made on the simple empty test object shown in Fig. 4.20. Here, three POEs of equal size couple to a single wire inside a single cavity. This object is very much like the object studied in [1]. Fig. 4.21 shows the far-field

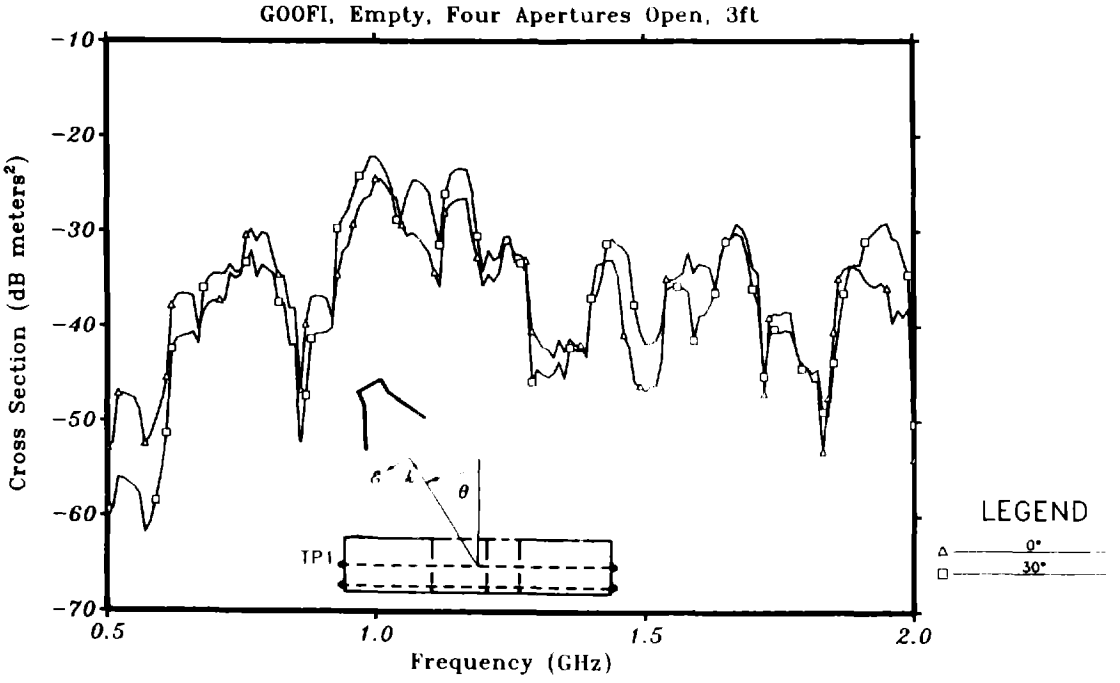

Fig. 4.18. Receiving cross-section for four centermost apertures when the source antenna aperture is 3 ft. from the object center. The parameter is the angle of incidence, $\theta = 0$ and 30°. Empty. TP1.

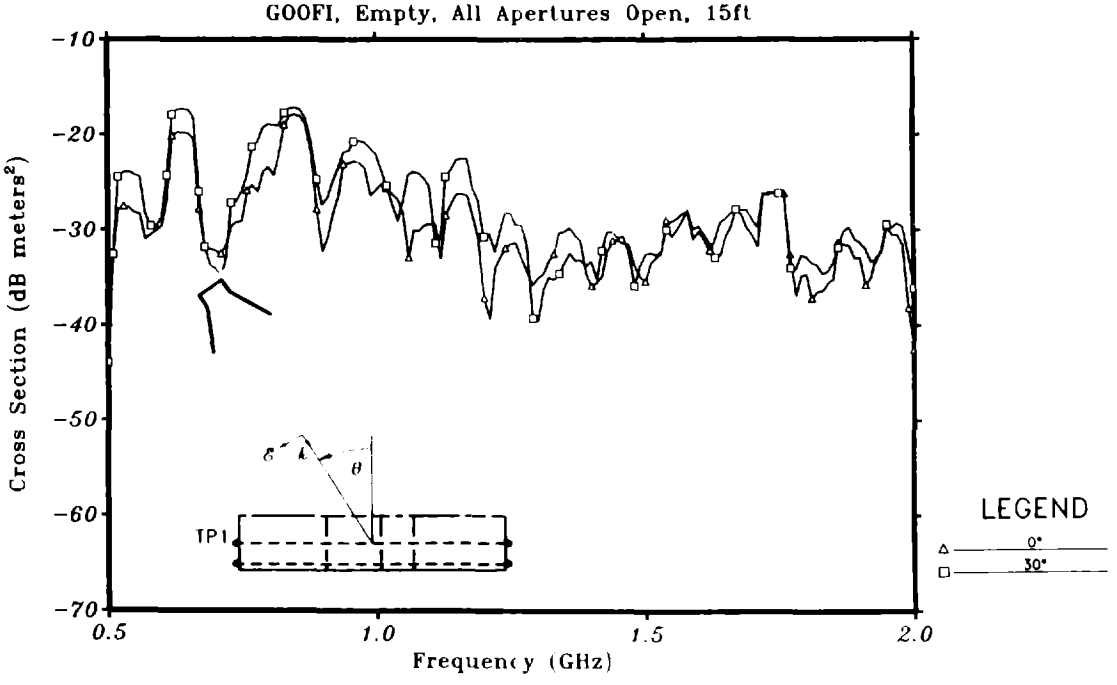

Fig. 4.19. Far-field receiving cross-section when all eight apertures are open. The parameter is the angle of incidence, $\theta = 0$ and 30°. Empty. TP1

receiving patterns for this object at 3.22 GHz with the bottom (i.e., nearest to the coupling terminal) POE open only, the middle POE open only, and all three POEs open simultaneously. Notable observations are the nearly omnidirectional coupling over the $\pm 90^{\circ}$ sector when only one POE is open, the fact that single POEs have similar contributions, and finally the strong constructive and destructive interference when all three POEs are open simultaneously. This later feature derives from the nearly equal contributions of the three POEs along with the variation of the phase of the incident field as the angle of incidence is changed.

Clearly, in this highly idealized and deterministic case having few random features, the phase of the incident field is very important. Consequently, illuminating such an object in the near-field of a source antenna will certainly not create the same receiving cross section as if the object were illuminated by a plane wave.

In summary, we have seen that coupling via multiple POEs is comprised of two parts; a deterministic or coherent part (generally resulting from the contributions of a few dominant POEs), and a more or less stochastic or incoherent part (resulting from the contributions of several lessor contributing POEs) superimposed on the dominant part. The deterministic part is highly sensitive to simultaneous excitation of two or more dominant POEs with the proper amplitude and phase, i.e., spot size. The stochastic part is much less sensitive to the phase of the incident field.

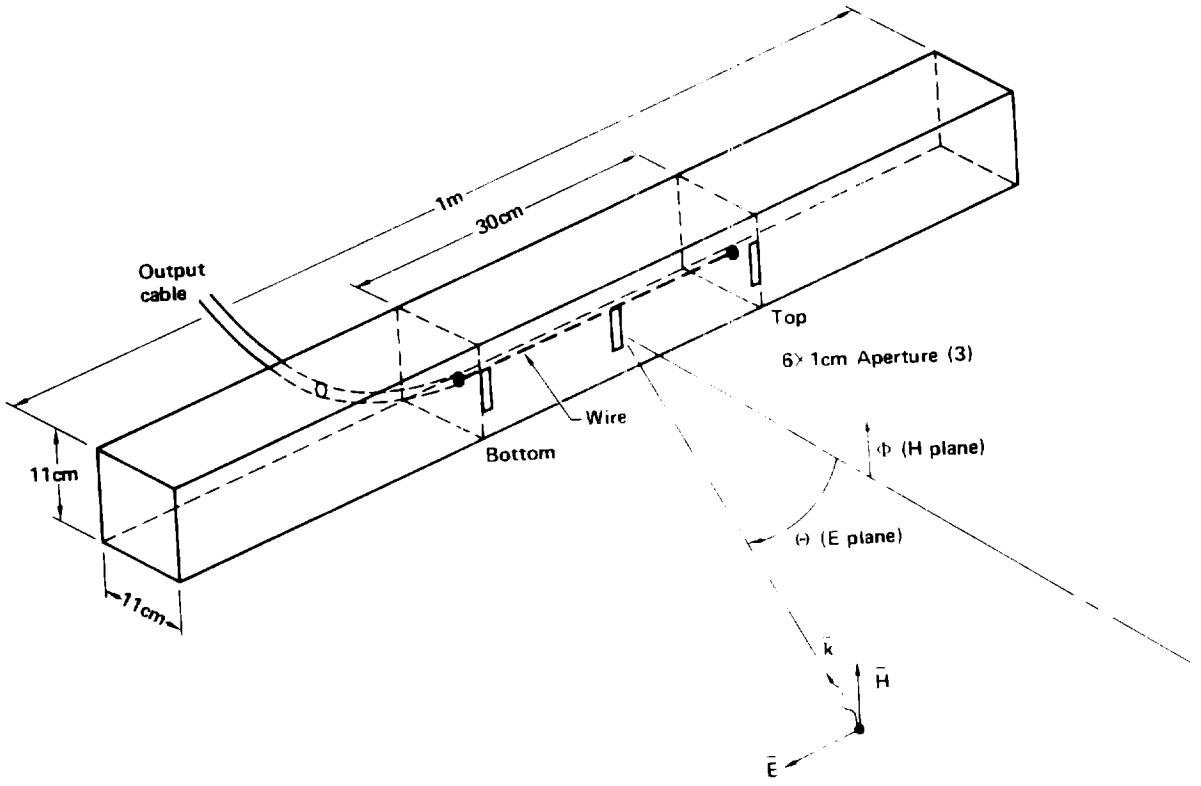

Fig. 4.20. Test object having three equally sized and spaced POEs which couple to a single wire inside a single cavity.

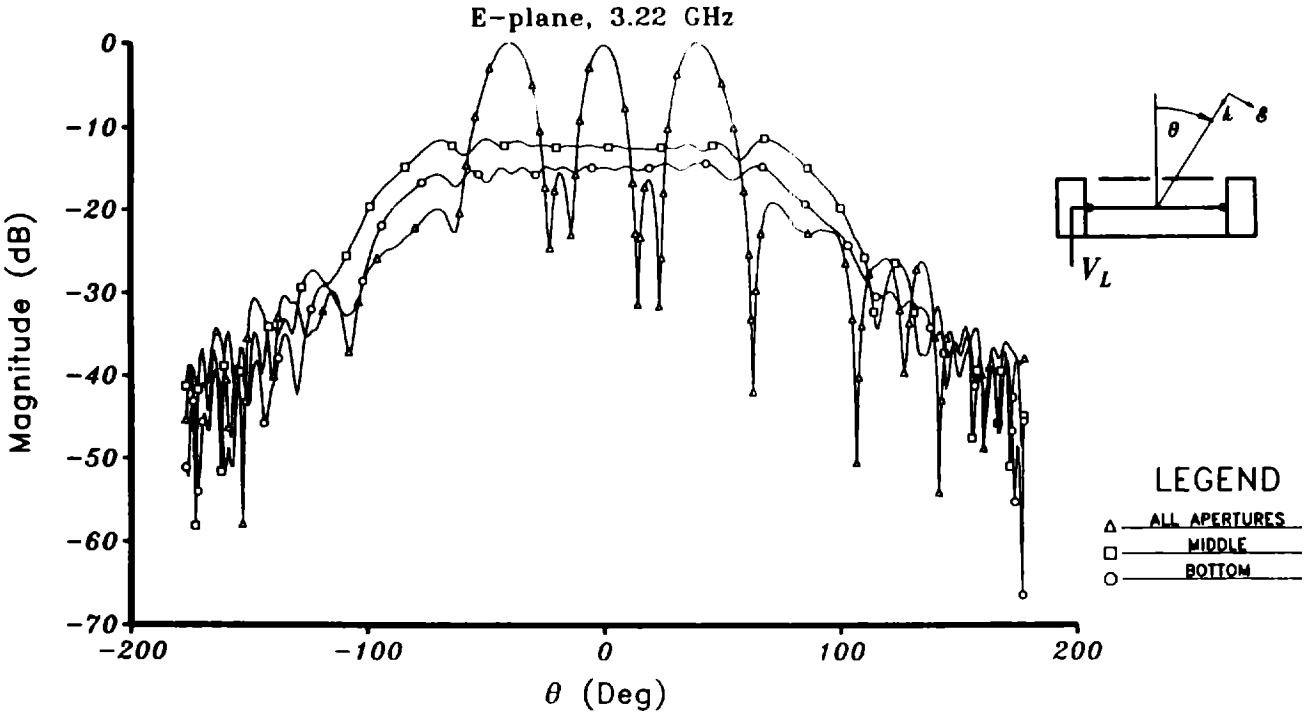

Fig. 4.21. Far-field receiving patterns for the test object shown in Fig. 4

4.5 Effects of Hardware Fill

As noted at the end of Sec. 3, the coupling to the test object of Fig. 3.1 was measured in its empty state and when its four compartments were randomly filled with scrap hardware consisting of various pieces of electronics, dielectrics, wires, cables, and microwave absorbing materials (Fig. 3.4). Examples of data in which the object was both empty and filled have already been given in the previous sections. From these, the reader has probably noted the distinctly different overall behaviors for these two situations.

For example, comparing Figs. 4.6 (empty) and 4.8 (filled) we see that the coupling level and degree of constructive and destructive interference is much greater when the object is empty than when filled. Fill also has the effect of smoothing the response, i.e., the Q-factors at the resonances are noticeably reduced. Adding fill also increases the randomness of V_n, due to additional scattering within the object. Consequently, the average near-field receiving cross section for a filled object better approximates the true (far-field) receiving cross section, σ_t, (see Fig. 4.11). Aside from this later fact, whether an object is empty or filled has little to do with how the test object should be placed in the near- or far-field of the source antenna. Whether the object is empty or filled is chiefly of phenomenological interest. The following examples explicitly point out some of the unique differences. The results and conclusions given here are consistent with that reported in [1].

In Fig. 4.22, the near-field (1 ft.) coupling to TP1 via POE 1 (which is closest to TP1) clearly shows the damping effect (reduced resonance detail) due to the added fill material. Also, note the slightly reduced level compared to the empty object. Coupling to TP1 via POE 8 is shown in Fig. 4.23. In this case, the coupled signal must travel the entire length (2.44 m) of GOOFI to reach TP1. The fill causes the signal to suffer much more loss in propagating this length, due to increased scattering and dissipation encountered over this path. Thus, when an object is filled, coupling via a POE which is closest to the measurement terminal is expected to dominate.

Similarly, Figs. 4.24 and 4.25 show the coupling to TP3 via POE 8 (closest to TP3) and POE 1 (furthermost from TP3). Although not shown here, other POEs between 1 and 8 suffer less loss in proportion to their distance from the TP being measured, as expected.

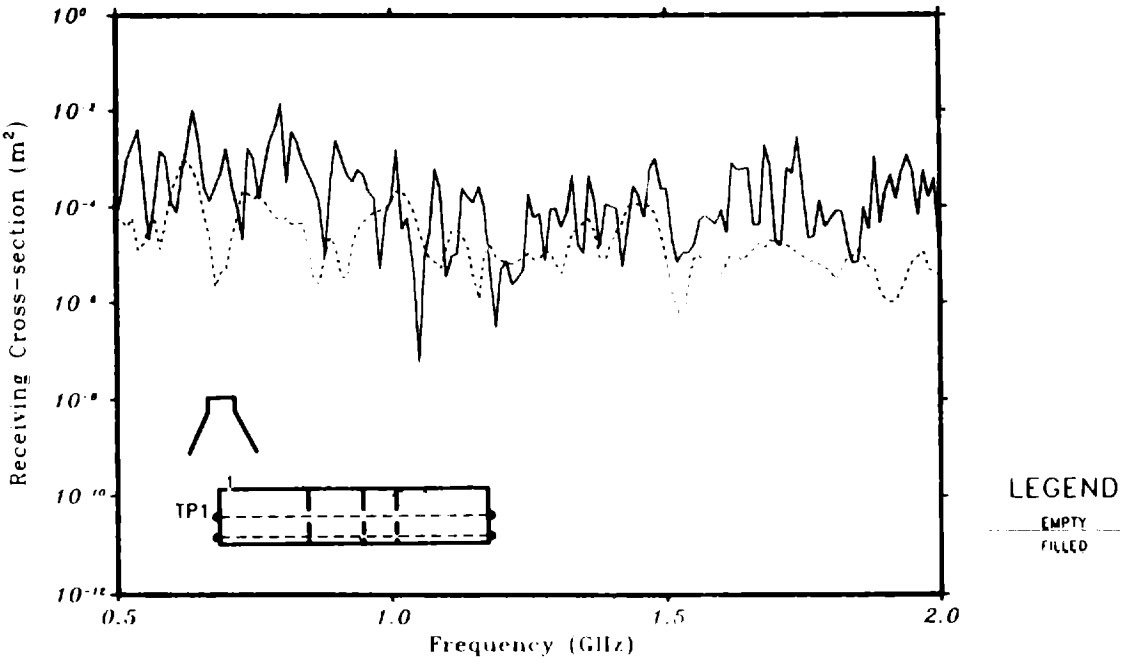

Fig. 4.22. Near-field (1 ft.) receiving cross-section of POE 1 as measured at TP1.

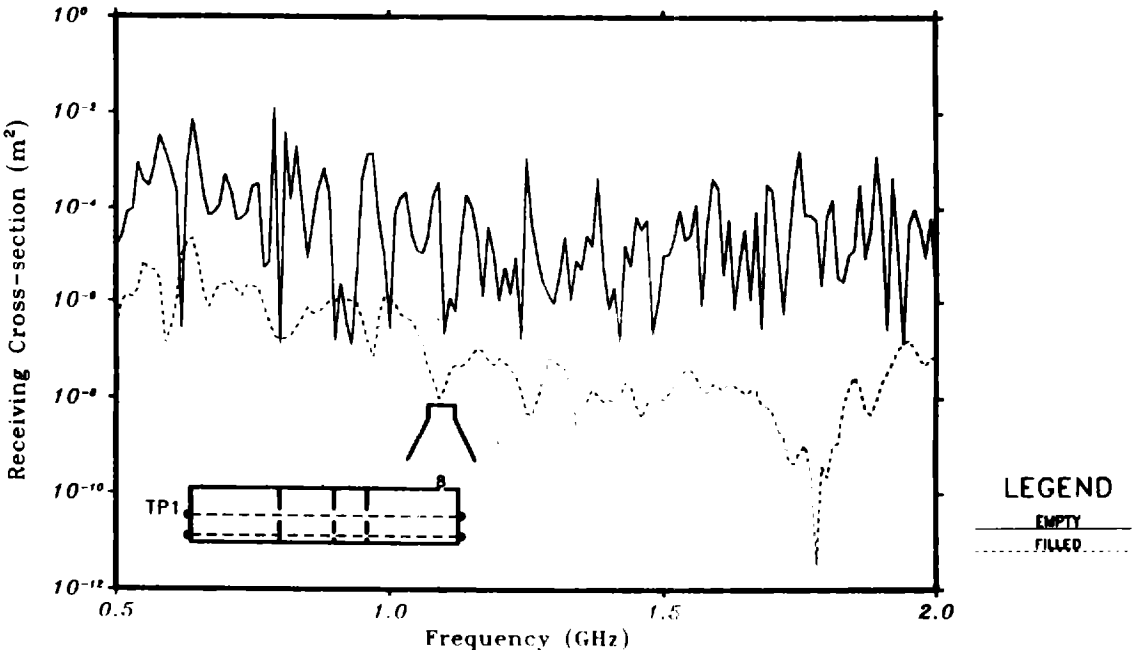

Fig. 4.23. Near-field (1 ft.) receiving cross section of POE 8 as measured at TP1.

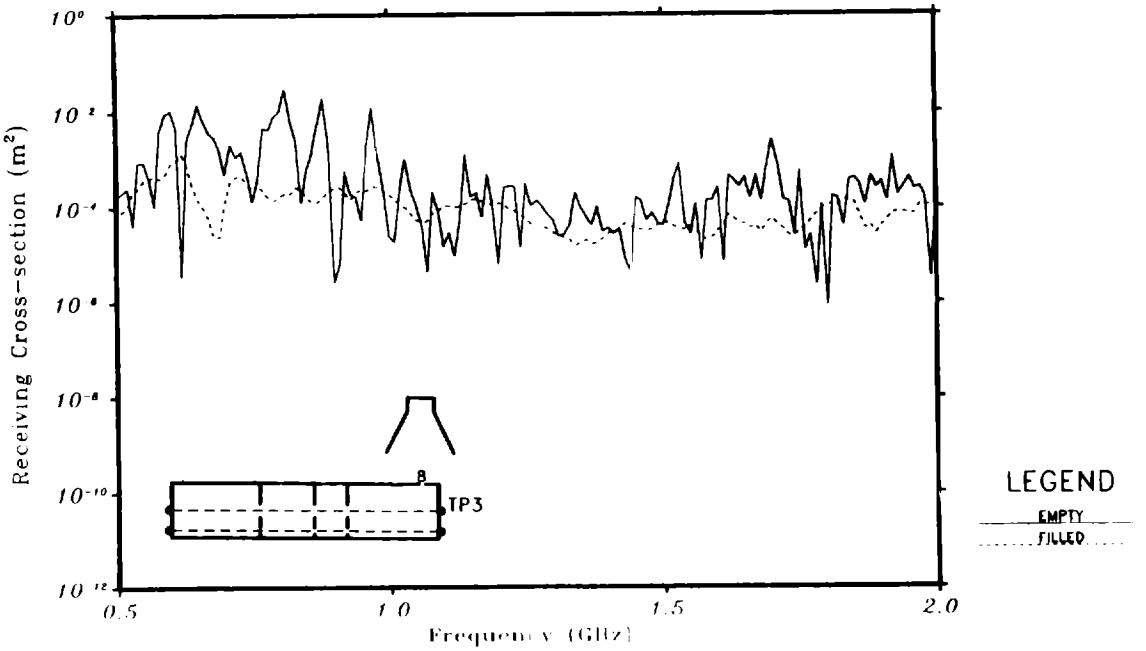

Fig. 4.24. Near-field (1 ft.) receiving cross section of POE 8 as measured at TP 3.

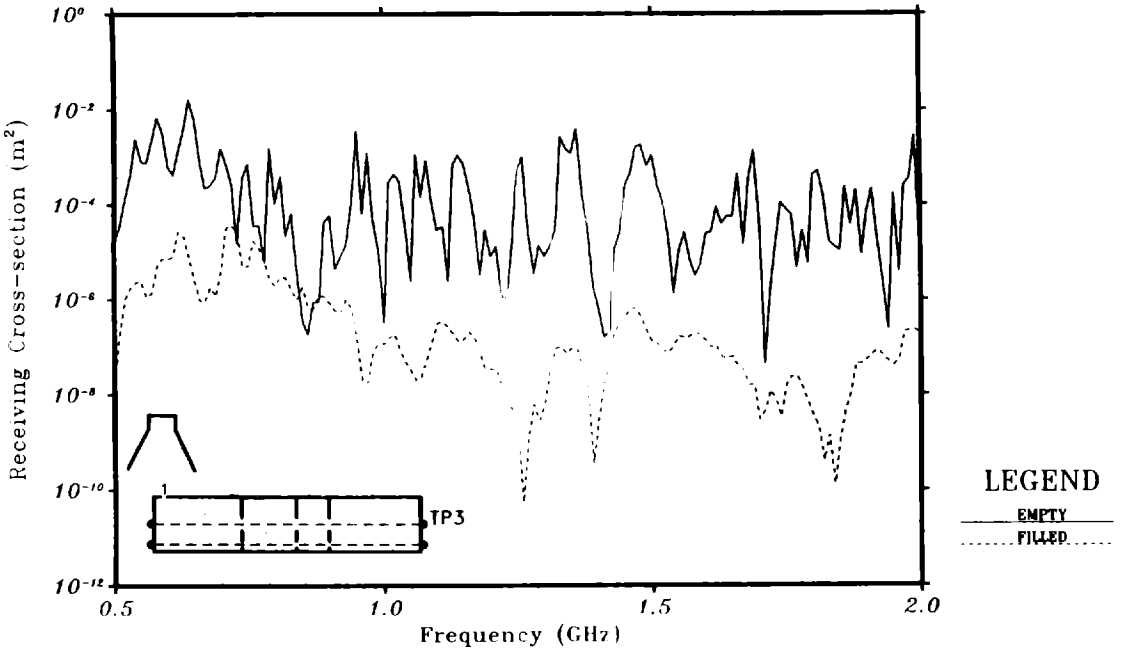

Fig. 4.25. Near-field receiving cross section of POE 1 as measured at TP3.

To further illustrate the relative importance of the several POEs according to their size and distance from the test point, consider Figs. 4.26 and 4.27 (filled) and Figs. 4.28 and 4.29 (empty). In these data the near-field (1 ft.) contributions of all eight POEs were measured individually and summed, $(\Sigma\sigma_n)_{1\ ft.}$, as was done in Sec. 4.2. Then, the contributions of each individual POE was ratioed to the total over the $0.5 \rightarrow 2$ GHz frequency range. The results are graphically shown in these figures. Further, contributions of the individual POEs were integrated over frequency, and ratioed to the sum of the integrated contributions. This ratio (in percent) which corresponds to the fractional energy contributed by each POE relative to the approximate total energy of all eight POEs is given in the upper right-hand corner of each figure.

Comparing Figs. 4.26 and 4.27 the amount of attenuation suffered by the signal at TP1 due to POE 8 in the filled object is obvious. POE 1, which is closest to TP1, contributes significantly over several sub-bands of the total frequency span and it contributes 45.1% of the total energy. POE 8, which is furthermost from TP1, contributes only 1% of the total energy, and this only occurs over a few of the lower frequencies.

In contrast, the data in Fig. 4.28 and 4.29 were taken under the same circumstances except that GOOFI is empty. Now, POE 1 is seen to contribute less fractional energy (26.5% compared to 45% when filled; see Figs. 4.26 and 4.28), and does so over much narrower frequency ranges. From Figs. 4.29 and 4.27, POE 8 contributes 12.1% fractional energy when empty (compared to 1% when filled), and does so in narrow bands over the entire frequency span. In these examples, the effects of fill are striking.

Table 2 compares the fractional (in percent) energy contribution of each POE relative to the total energy contributed by all eight POEs when GOOFI is filled and empty. Data is given for TP1 and TP3.

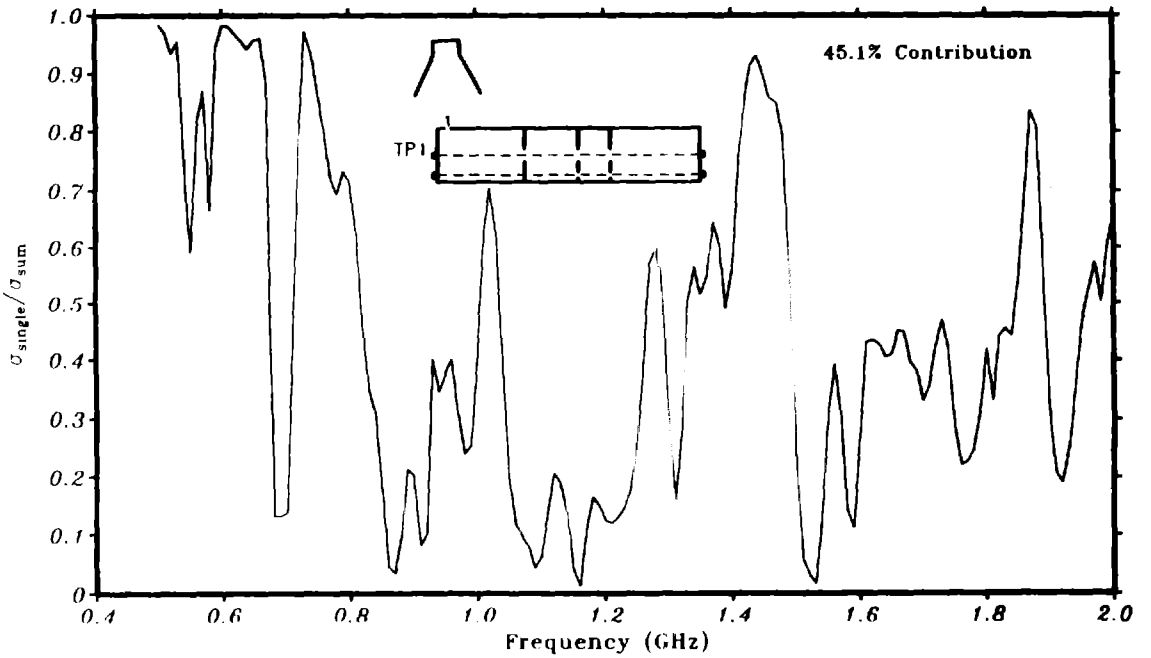

Fig. 4.26. Near-field contributions of POE 1 only $(\sigma_1)_{1\ ft.}$, relative to the incoherent sum of all eight POEs $(\Sigma\sigma_n)_{1\ ft.}$, as measured at TP1 when GOOFI is filled.

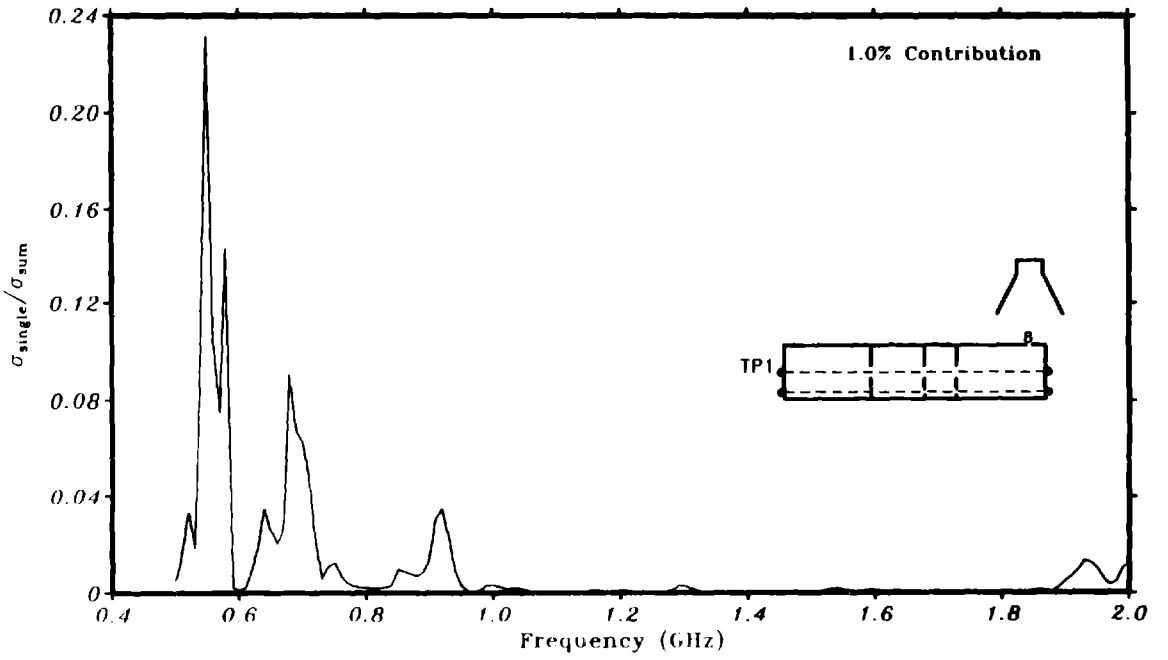

Fig. 4.27. Near-field contributions of POE 8 $(\sigma_8)_{1\ ft.}$, relative to the incoherent sum of all eight POEs $(\Sigma\sigma_n)_{1\ ft.}$ as measured at TP1 when GOOFI is filled.

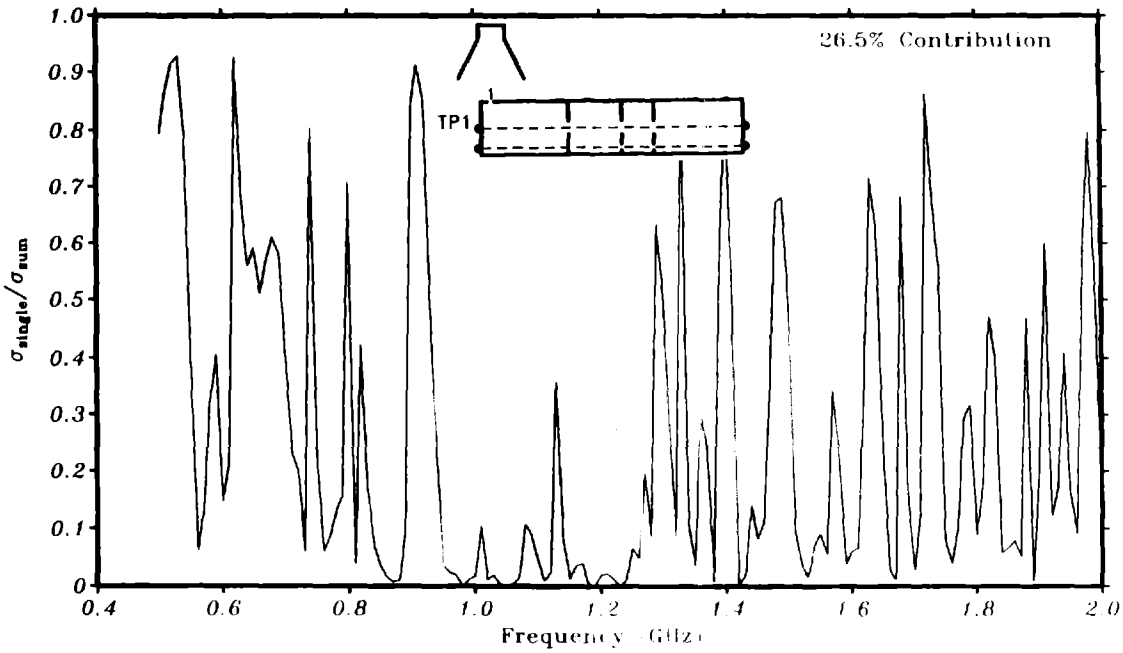

Fig. 4.28. Near-field contributions of POE 1 only $(\sigma_1)_{1\ ft.}$, relative to the incoherent sum of all eight POEs $(\Sigma\sigma_n)_{1\ ft.}$, as measured at TP1 when GOOFI is empty.

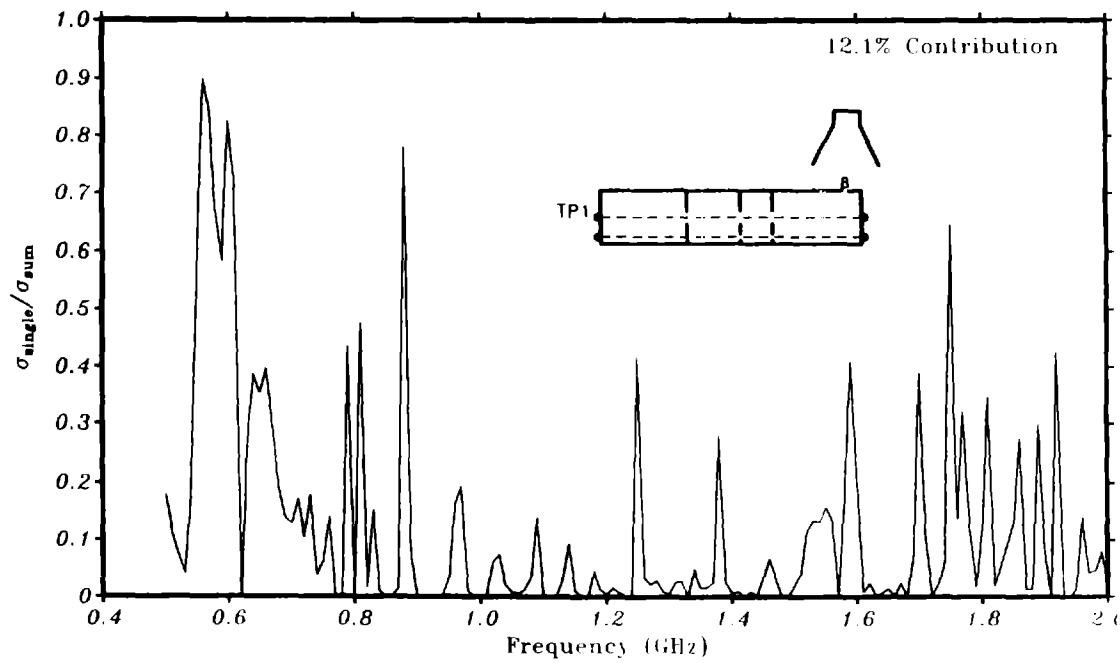

Fig. 4.29. Near-field contributions of POE 8 $(\sigma_8)_{1\ ft.}$, relative to the incoherent sum of all eight POEs $(\Sigma\sigma_n)_{1\ ft.}$ when GOOFI is empty.

Table 2

	TP1		TP3	
POE#	Filled	Empty	Filled	Empty
1	45.1%	26.5	.6	14.5
2	34.4	19.9	.3	6.27
3	.05	.2	.002	.053
4	8.0	5.5	.4	4.15
5	3.1	16.9	1.4	14.37
6	5.8	9.5	2.5	12.55
7	2.5	12.1	24.2	21.58
8	1.0	12.1	70.5	26.44
Total	99.95%	102.7%	99.9%	100.41%

To summarize this section, filling an object has the effect of:

(a) Substantially reducing the coupling level to a given terminal or pin in proportion to the distance from the POE to the terminal or pin, especially at the higher frequencies.

(b) Substantially reducing the coupling level compared to the same object when empty.

(c) Decreasing the sharpness of internal resonances and other constructive and destructive interferences (reduced Q-factors).

(d) Making the near-field receiving cross section more nearly approximate the true or far-field receiving cross section, σ_t, due to the smoothing effect of (c).

5. Conclusions

This study clearly points to the need for low level cw characterization of a test system in order to understand the roles that each of several POEs can play. The frequencies at which each POE contributes significantly is particularly important as is also the dependence on incidence angle, but to a lesser degree over certain sectors depending on the POE receiving pattern. Although polarization of the incident field was not considered here (because the POEs in the test object used all respond to the same polarization) its effect also deserves characterization. This would be particularly important when testing an object having several POEs at different polarizations, or an object having unobvious POEs or unknown polarizations. This is an effect deserving of further study.

Low level characterization allows one to determine how the near-field coupling compares to far-field coupling, thereby giving insight as to the approximations and risks taken in doing susceptibility testing in the near-field of an HPM source antenna. Armed with the knowledge of which POEs are dominant, and the frequencies, angles of incidence and polarizations over which they are dominant, allows the HPM test to be designed and carried out with good judgement.

Not only should the coupling to the test object be characterized, but the source antenna itself should also be characterized to determine its antenna factor vs. frequency and to insure that its near-field pattern is properly shaped (spot size) and polarized. Besides giving information concerning the behavior of the near-field, the data (which are the incident intensities) will be used to normalize coupling measurements made inside the test system.

The results of Secs. 4.1 and 4.2 have shown that the near-field receiving cross section compares quite favorably with the far-field cross section, provided that the near-field spot size is large enough to illuminate all of the important POEs simultaneously. These results also show that the near-field receiving cross section can be calculated in the same manner as is conventionally done for the far-field cross section (see eq. (5)). This can be done using the incident field as measured on boresight of the source antenna in its near-field in the absence of the test object.

Coupling via multiple POEs is comprised of two parts; a deterministic part (generally resulting from coherent contributions of a few dominant POEs), and a more or

less stochastic part (resulting from the contributions of several lessor contributing POEs) superimposed on the deterministic part. The deterministic part is highly sensitive to simultaneous excitation of two or more dominant POEs with proper amplitude and phase, i.e., spot size. The stochastic part is much less sensitive to the phase of the incident field.

Secs. 4.2 and 4.3 has also shown that for multiple POEs, the trend of the true far-field receiving cross section is well approximated as the incoherent sum of the near-field receiving cross sections, $\Sigma\sigma_n$. Such a scalar sum, however, obviously cannot account for destructive interferences because of the lack of any phase information. It also slightly overestimates of the true far-field receiving cross section (see Figs. 4.8-4.11).

For these same reasons, if the phase of the incident field which excites the important POEs deviates from that of a plane wave, the coupling details at frequencies where constructive and destructive interferences occur become blurred, but the receiving cross section trend is relatively unchanged (see Fig. 4.17).

Sec. 4.3 further considers the coherency of contributions from the individual POEs. Here, it is demonstrated that the cumulative response is indeed coherent, and that this coherency must be maintained by the incident field if all of the detailed features (destructive interferences) are to be accurately captured. If such detailed accuracy is needed, it is necessary to illuminate the most important part of the whole system simultaneously. This should be done using a source having a spot size which is sufficient to excite all the important POEs with their proper amplitude and phase. As noted earlier, amplitude and phase distributions which do not approximate a plane wave tend to blur the points of constructive and destructive interference.

But if only the average response is sufficient, the incoherent sum $\Sigma\sigma_n$ is adequate. Finally, the incoherent sum $\left(\Sigma\ |V_n|\right)^2$ gives an upper bound to the total coupling cross section, as if all voltages were in phase (a highly unlikely situation).

Coupling to a single POE is generally quite insensitive to the angle of incidence. For multiple POEs having nearly equal contributions, coupling becomes highly deterministic and coherent. This may result in strong interferences (see Fig. 4.21). Although this condition is rather unlikely in a realistic system, if such a situation exists it is essential that the phase of the incident field approximate a plane wave. Hence, the object

should be located in the source far-field. Again, distortions of the incident field caused by placing the object in the source near-field will cause the constructive and destructive interferences to be blurred.

Filling an object with hardware, compared to when the same object is empty, reduces the average coupling, especially at the higher frequencies. This attenuation is proportional to the distance from the POE to the measurement terminal. The fill also has the effect of smoothing the response, i.e., the Q-factors of the resonances are substantially reduced. Although these effects are chiefly of phenomenological importance, there is one important consequence relative to near-field testing. Since the resonance are damped by the fill, the impact of additional blurring caused by placing the object in the source near-field is substantially reduced. Thus, the near-field incoherent sum $\Sigma\sigma_n$ better approximates the true or far-field coherent sum, σ_t, for filled objects.

References

[1] R. P. Toth and L. D. Bacon, "Microwave Coupling Inside Complex Systems," Sandia National Laboratories SAND86-1952, July, 1987.

[2] R. J. King and H. G. Hudson, "HPM Simulations Fidelity Studies", Lawrence Livermore National Laboratory, UCRL-97846, June 1988.

[3] K. S. Kunz, H. G. Hudson, J. K. Breakall, R. J. King, S. T. Pennock, and A. P. Ludwigsen, "Lawrence Livermore National laboratory Electromagnetic Measurement Facility", IEEE Trans. on Electromagnetic Compatibility, EMC-29(2), May, 1987, pp. 93-102.